THESIS

DEVELOPMENT OF A NOVEL ADDITIVE MANUFACTURING METHOD: PROCESS GENERATION AND EVALUATION OF 3D PRINTED PARTS MADE WITH ALUMINA NANOPOWDER

Submitted by

Tucker Joseph Hensen

Department of Mechanical Engineering

In partial fulfillment of the requirements

For the Degree of Master of Science

Colorado State University

Fort Collins, Colorado

Fall 2017

Master's Committee:

Advisor: John D. Williams
Co-Advisor: David A. Prawel

Quiang Wang

ABSTRACT

DEVELOPMENT OF A NOVEL ADDITIVE MANUFACTURING METHOD: PROCESS GENERATION AND EVALUATION OF 3D PRINTED PARTS MADE WITH ALUMINA NANOPOWDER

Direct coagulation printing (DCP) is a new approach to extrusion-based additive manufacturing, developed during this thesis project using alumina nanopowder. The fabrication of complex ceramic parts, sintered to full density, was achieved and the details of this invention are described. With the use of additive manufacturing, complex features can be generated that are either very difficult or unattainable by conventional subtractive manufacturing methods. Three unique approaches were taken to create a slurry suitable for extrusion 3D-printing. Each represented a different method of suspending alumina nanopowder in a liquid; a bio-polymer gel based on chitosan, a synthetic polymer binder using poly-vinyl acetate (PVA), and electrostatic stabilization with the dispersant tri-ammonium citrate (TAC). It was found that TAC created a slurry with viscosity and coagulation rate that were tuneable through pH adjustment with nitric acid. This approach led to the most promising printing and sintering results, and is the basis of DCP. Taguchi and fractional factorial design of experiments models were used to optimize mixing of the alumina slurry, rheological properties, print quality, and sinterability. DCP was characterized by measuring the mechanical properties and physical characteristics of printed parts. Features as small as ~450 μm in width were produced, in parts with overhangs and enclosed volumes, in both linear and radial geometries. After sintering,

these parts exhibited little to no porosity, with flexural modulus and hardness comparing favorably with conventionally manufactured alumina parts. A remarkable aspect of DCP is that it is a completely binderless process, requiring no binder removal step. In addition, DCP can employ nanopowders, allowing for enhanced mechanical properties as observed in nano-grained materials. Perhaps most importantly, any material that acquires a surface charge when in aqueous media has the potential to be used in DCP, making it a method of additive manufacturing using many metals and ceramics other than alumina.

ACKNOWLEDGEMENTS

A huge number of people have given their time and effort in helping me through graduate school, so I would like to thank them. To start, my past advisor, Troy Holland, always challenged me to understand everything about everything that I worked with in the AMPT Lab. Troy provided my first experiences with many of the instruments and practices that are essential to materials science, as well as exciting, advanced things like SPS and CEFAS machines. As a source of instrumental insight during this research, conversations with Troy were always noteworthy.

The PhD students of the AMPT Lab and MERC in general, gave sage wisdom, and fellow Master's students traded new tricks and theories. Both entertainment and competition were present, and great friendships, and paper edits, came of it. I wish the best of luck to Corson Cramer, Trevor Aguirre, Patrick Rodriguez, Jamison Bair, and Mark Bourgeois, and thank them for the memories.

Once moving into working with the CEPPE Lab under John Williams, my passions for space and materials science were blended in my work. John gave advice and wit freely, on old research, new research, crazy ideas, and simple problems. His support was invaluable in my writing this thesis, and provides constant inspiration.

The CEPPE Lab, Sapien, and Plasma Controls have all helped innumerable times in my research and my learning of plasma systems and ping pong equally. Daisy Williams was there for me with a solution for anything that I needed. Seth Thompson, Anna Kindvall, Ryan Ham, Bao Nguyen, and Kirk Boehm all helped teach me the basics of survival at the CEPPE Lab, from turning on a vacuum pump to plasma physics. Matt Schultz, JJ Moritz, and

Marco Martinez at Sapien, as well as Casey, Cody, and Sean Farnell of Plasma Controls were always a pleasure to work with.

I would also like to give special thanks to my co-advisor, Dr. David Prawel, who has provided technical support and encouragement since my undergraduate program. His Idea2Product lab first enabled me to explore 3D printing, and his graduate class gave me the fundamentals of 3D printing technology from its invention to what it has become today. From 3D printing a clock to career advice, David's input was always of great value.

My committee member, Professor Qiang (David) Wang, gave insightful technical help with understanding colloid science, and was very helpful. Outside my committee, Professor Kaka Ma provided excellent edits for my papers, and great advice in research and academia. Dr. John Chandler has helped me see what I could never see before, under the electron microscope. His teaching has led to a wealth of information and stunning micrographs.

Finally, and most importantly, I would like to thank my friends and family. Friends, thanks for the constant distractions and glimpses into other perspectives, as well as the favors and the memories. As for family, my parents, Frank and Ruth Hensen, have been role models and motivators throughout my education; I could never have achieved this without them. My sister, Rachael, has always been a great source of friendship and inspiration, with a perspective looking right into the blind spots in mine.

TABLE OF CONTENTS

LIST OF TABLES

LIST OF FIGURES

LIST OF EQUATIONS

1 Introduction

Here, the impetus for this thesis research is presented. This is followed by a background and summary of approaches to achieving the ultimate goal. An overview of related theories is presented. The introduction concludes with an outline for the rest of the thesis.

1.0 Specific Aims

This research set out to accomplish three specific aims concerning designing a material system and method for ceramic additive manufacturing (AM).

First, a slurry had to be developed with the requirements that it is extrudable, material independent, and with a solids content sufficiently high to be printed in near net shape and sintered to a high degree of relative density. In other words, to be extrudable, the material had to be able to flow through a nozzle, and cease flowing almost immediately afterward. To achieve material independence, the fundamental suspension mechanism must be able to be applied to a broad selection of materials. A high solids content is essential to minimizing shrinkage, and achieving full density allows comparison of parts from this method to those produced by conventional methods.

Second, parts had to be made demonstrating complex geometry. Essentially, this covered any feature that would be extremely difficult or simply impossible without additive manufacturing, especially overhangs and enclosed features.

Finally, the sintering of the material had to be optimized. This extended to the production of fully dense (>97% theoretical density) parts with complex geometries.

The culmination of these specific aims was the development of a novel, relatively low cost, and adaptable method of AM, competitive with current methods.

1.1 Processing and Manufacturing of Ceramics

This section introduces the various technologies upon which this research is founded. From conventional methods to advanced additive techniques for ceramics, a basic overview is given, with references, which offer excellent background and fundamental knowledge for the curious reader.

1.1.1 Conventional Methods

Some conventional methods of making ceramic parts have been around since ancient times, such as clay suspensions and slip casting, while others such as gas, liquid, and powder precursor methods were developed more recently [1]–[6]. Typically, the initial forming process is the most critical stage because ceramics do not machine well and many require expensive tooling due to their inherent brittleness and low fracture toughness. In many cases where a complex geometry is required, the post-hard machining of ceramics can account for 80% of the total cost [4]. Hence, many ceramic parts are designed with geometries that are possible through casting or film deposition. This limits the possible geometries and also increases overall cost of manufacturing by requiring tooling or chambers with tight environmental controls. A comprehensive background on conventional and recent ceramic processing is beyond the scope of this work, but can be found in references [1], [5].

1.1.2 Additive Manufacturing (AM)

As with many other materials, additive manufacturing of ceramics offers the potential for enormous expansion in capability and creativity in design [7]. AM, in general,

relies on the principle of bottom-up or inside-out design styles for manufacturing, using point, line, or areal material placement. AM was originally developed using thermoplastics, and has since expanded to include techniques for all types of plastics, biomaterials, metals, ceramics, electronics, and composites of nearly all of the above. Examples of many of these various technologies are show in Figure 1 from reference [4].

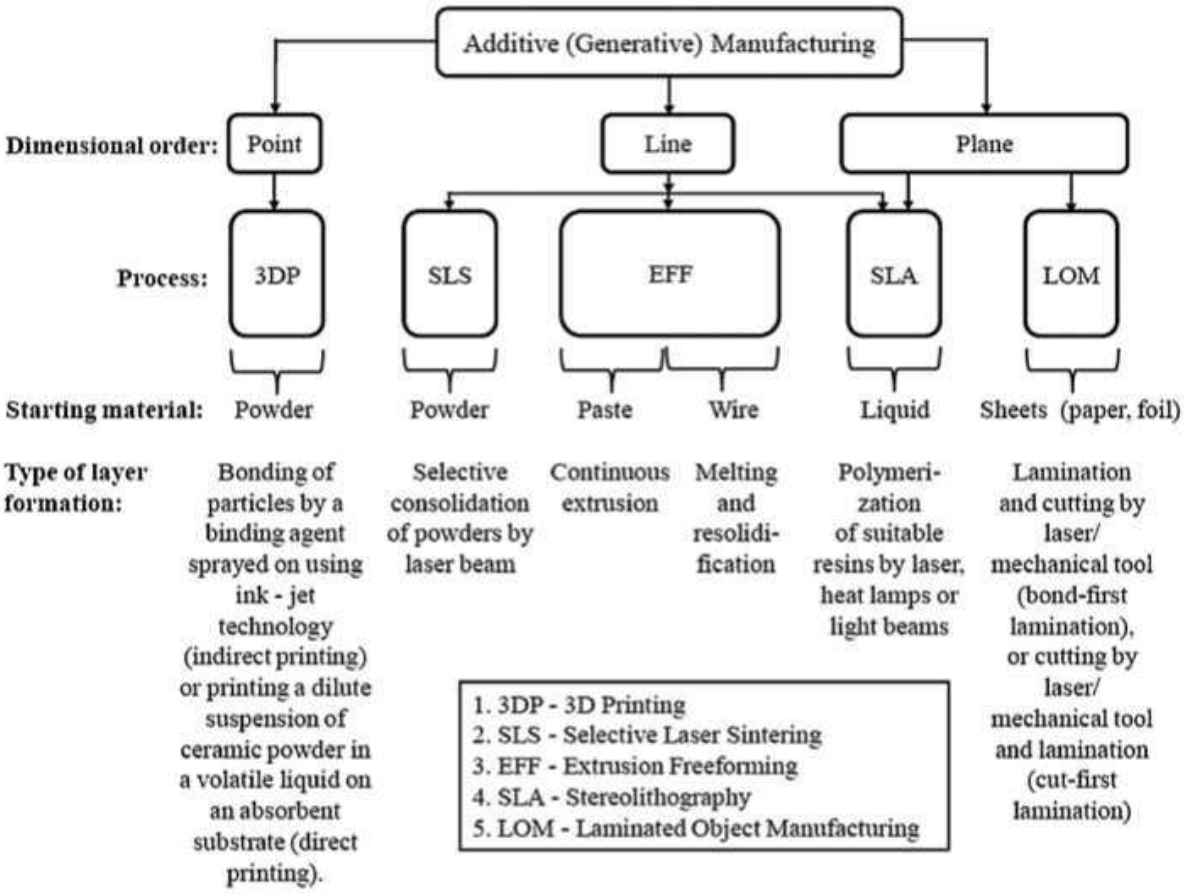

Figure 1: Classification of AM processes according to dimensional order [4]

The various additive technologies each offer advantages for specific geometries, material systems, and desired properties. All of the extrusion freeform (EFF) technologies depend on a system with 3-axis motion capability and some form of material dispensation, such as a common extrusion-based printer used for EFF and shown in Figure 2.

Figure 2: Lulzbot Taz 6 extrusion-based printer for thermoplastics

Some other technologies, such as lithography-based solutions, laser melting, and binder jetting systems use a vat or bed of material and perform processes to isolate that which is desired, while the rest is removed in post processing. Some of these techniques can produce parts requiring little to no surface finish operations, with resolution down to the nano-scale [8]. In contrast, many of the extrusion-based hobby printers such as the Lulzbot Taz 6 are sold with nozzles typically enabling 200 - 500µm minimum feature size. The quality of parts from the low-cost extrusion printers has been shown to be adequate for many functional research and general practical purposes, as evidenced by the many forums and CAD sharing websites dedicated to them (thingiverse.com, 3ders.org, 3dhubs.com, forum.lulzbot.com etc…). AM has been applied to the manufacture of nearly everything imaginable, from art to hand tools to FAA certified aircraft components.

1.1.3 Additive Manufacturing of Ceramics

The progress of ceramic additive has been slower to advance than that of metals or polymers, partially due to the extreme physical properties of ceramics [6]. Regardless, functionalized ceramic parts such as piezoelectrics [4], multi-material composites [9], refractory heat exchangers [10], biomedical implants [4], [11], and structural components [12] have already been produced, to name a few.

Of the multitude of additive techniques available, a remarkable amount have been adapted with the ability to make ceramic parts. Those techniques that have been replicated with ceramic and the differences between them are illustrated in Figure 3 from reference [3]. While these techniques have all been shown to produce parts, not all have proven the quality or reliability for functional applications.

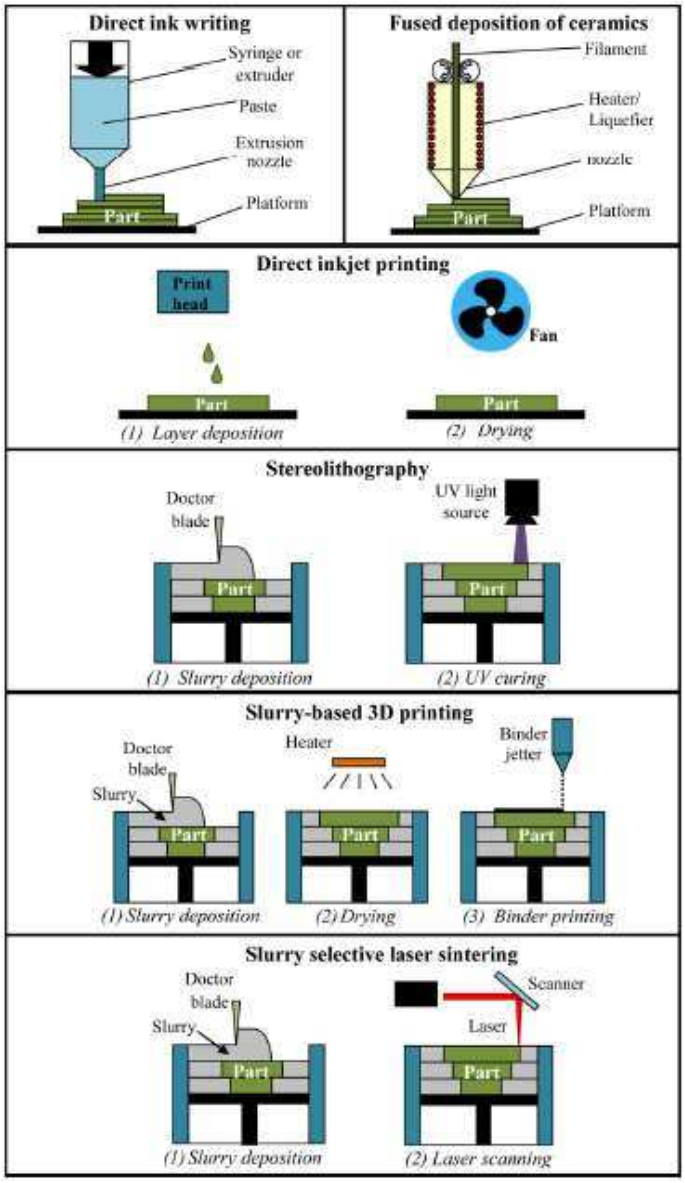

Figure 3: Powder and colloidal suspension-based ceramic additive techniques [3]

For the scope of this research, special attention is paid to the direct ink writing (DIW) family of processes. All of the methods investigated used an unheated syringe to extrude a paste in layers, which then solidifies, onto a substrate. In these extrusion-based styles of additive, the extrusion behavior of the paste defines the maximum possible quality of the part. This can be seen in Equation 1, from [13], where ΔP is the required extrusion

pressure, Q is the volumetric flow rate, μ is viscosity, l is the nozzle length, r is nozzle radius, and σ is surface tension.

$$\Delta P = \frac{8Q\mu l}{\pi r^4 \sigma}$$

Equation 1: Required Extrusion Pressure

Required extrusion pressure is proportional to viscosity, and inversely so with respect to surface tension. An extruder is normally limited by the maximum pressure that can be generated under the power of the motor and reduction of the transmission. With this as a constraint, an increase in viscosity requires a proportional increase in pressure to avoid clogging or other failure. On the other hand, an increase in surface tension could potentially be used to counteract this effect. On a very general level, there are a few considerations necessary when extruding powder suspensions; namely the amount of powder by volume fraction, and the physical characteristics of the powder. To print parts with tolerable shrinkage and capability to be sintered to full density, it is suggested that powder volume fractions are at or above 50 vol% [14]. Viscosity is naturally raised with higher powder concentrations due to more frequent particle collisions and friction, such that ultra-high powder concentrations such as 80 vol% may be too viscous to print without expensive, high-pressure extrusion systems. When attempting to extrude with very fine resolution, a very small nozzle is desired. As a general rule, the size of the particles in suspension must be at least 50 times smaller than the nozzle to allow for the approximation of fluid flow characteristics and to avoid clogging. For example, if using a powder with average diameter 150 nm, the minimum nozzle diameter is 7.5 μm. Furthermore, the suspension must typically be modified to ensure structural stability of the

final part. This is usually done with the addition of dispersants, binders, and plasticizers of various sorts, with as much as 7 wt% of impurities, as shown in a comparison of constituents between two suspension-based ceramic additive techniques in Figure 4 below. Purity of ceramics is typically of critical importance for producing the intended properties. If such impurities are not thoroughly removed, parts may be highly unreliable.

The characteristics of the specific methods and suspension mechanisms investigated for this research are described in the following section.

Component	*Function*	*Classical tape casting slurry containing solvents (wt%)*[10]	*Typical tape casting slurry using UV curable binder (wt %)*
Alumina	Ceramic powder	67·4	82
MEK/EtOH	Solvent	25·6	
Phosphate ester	Dispersant	0·5	0·8
Polyvinylbutyral	Binder	2·7	
Dibutyl phthalate	Plasticizer	1·8	
Polyethylene glycol	Plasticizer	2	
Polyester acrylate	Photopolymerizable binder		15·2
2-hydroxy-2-methyl-1-phenyl-propan-1-one	Initiator		2

Figure 4: Comparison of suspension constituents for different ceramic additive techniques

1.1.4 Investigated Suspension Types

The following methods of particle suspension are discussed with respect to function with colloidal particle sizes. A colloid can be defined as a particle, upon which the Van der Waals and electrostatic forces in an environment can overcome gravitational forces, enabling indefinite suspension of particles without settling. Across many materials, colloidal particle sizes have a maximum around 10 μm. These suspensions often exhibit non-Newtonian behavior, and may be tuned to act as either a solid or a liquid. The different methods of particle suspension are discussed here.

Chitosan Gel

The first method to be tested was a rapidly crosslinking bio-polymer gel, with the hypothesis that the quick transition from liquid to solid could be well suited to extrusion printing. The process of gelation generally involves a polymer that is dissolved in liquid, which stiffens to form a semi-rigid structure when a crosslinking agent is introduced. This crosslinking agent induces bond formation between the dissolved polymer chains and the "crosslink" chemical chains. This bonding forces the polymer and crosslinking agent to form a solid network. This network can function as a matrix, capable of supporting other materials such as nanopowders, and the transition from liquid slurry to solid gel can occur in a matter of seconds. The procedure in this research is based off the work of Mekhail et al, [15] using the chemical guanosine 5'diphosphate (GDP) as a crosslinking agent for the bio-polymer chitosan. A drawback of this approach was found to be that the gel network necessitated a significant amount of impurities which could be very difficult to remove completely.

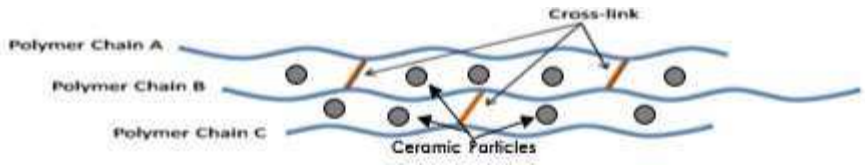

Figure 5: Diagram of a gel network suspending nanoparticles

PVA Binder

In an effort to create a slurry with sufficiently high viscosity to retain printed geometries, while involving a smaller amount of impurities, the synthetic polymers ammonium polyacrylate and polyvinyl alcohol (PVA) were investigated. Ammonium polyacrylate (Darvan 821-A, Vanderbilt Minerals LLC, USA) was used as a dispersant to

achieve high solids loading in the slurry. This product is designed for stabilization and improved solids content for ceramic suspension, and has been used frequently in literature [16]–[20]. PVA has been employed often in ceramic suspensions as a binder, and is frequently used in the production of adhesives, forming polyvinyl acetate, and in the thickening of other adhesives [5], [21].

Both the Darvan and the PVA binder have functional groups that bond to the alumina particles through dipole interactions, similar to ionic interactions. When these two are used in conjunction, the Darvan allows for high solids loading and the PVA provides the binding effect, raising viscosity to a point at which shape can be retained after extrusion or deformation. Depending on the concentration of the two constituents, the material system could be electrostatically, sterically, or structurally stabilized. The difference between these stabilization types is elucidated in Figure 6 below. Further clarification for ceramic colloidal suspensions and the stabilization types can be found in a summary provided by Lewis [2].

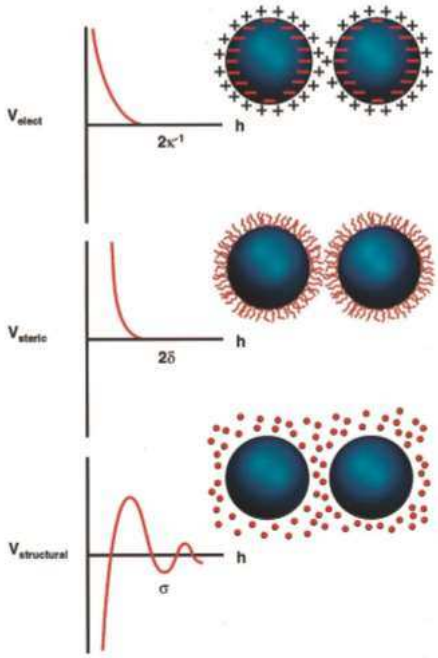

Figure 6: Diagram of a two-particle interaction and plots of the interatomic forces between them for (top to bottom) electrostatic, steric, and structural stabilization[2].

Direct Coagulation

For the proposed research, coagulation was shown to be the superior method of solidification of a liquid suspension, making it the best choice for the new extrusion printing method. This mechanism is based on the electrochemical reactions between the liquid solvent, the solid particles, and the coagulating agents added to the mixture. When particles are suspended in a liquid, the ions in the liquid adsorb onto the surface of the particles, leading to a surface charge on the particles and the subsequent creation of an electrical double layer around them. This leads to interparticle repulsive forces that are responsible for homogenous distribution in suspension. When a counter-ion is introduced, such as by a coagulant, or the pH of the suspension is shifted, this can lead to a reduction in the interparticle repulsion. This allows particles to flocculate and eventually form a solid coagulated structure, as shown in Figure 7. For the desired applications, the coagulation time is crucial to the design and it must be optimized for the additive manufacturing

process. This research shows that direct coagulation using triammonium citrate (TAC) salt as both dispersant and coagulant allows for a tunable coagulation rate, giving coagulation times from the range of seconds to minutes.

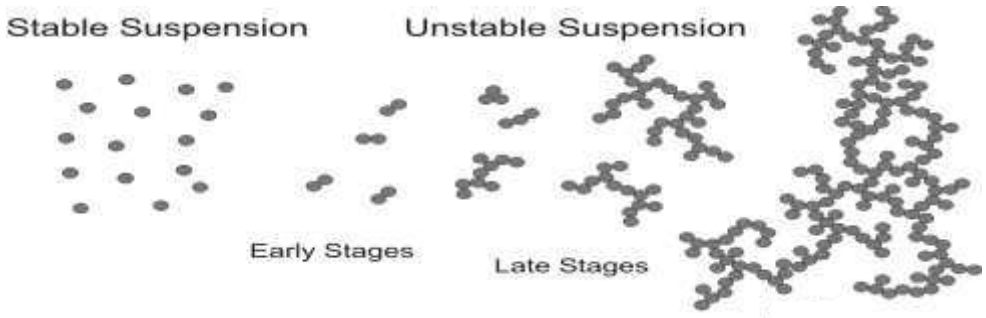

Figure 7: Stages of the coagulation process

The use of TAC in ceramic suspensions as a dispersant is documented in research [22]–[24]. The presence of adsorbed citrate and ammonium ions creates electrostatic stabilization. The direct coagulation printing process discussed in Chapter 3 presents a completely binderless method of extrusion printing, eliminating the need for a binder removal step as well as a significant reduction in impurities. To better understand the mechanisms behind the initial stabilization and subsequent coagulation, a discussion of the governing theory of electrostatic colloidal stabilization is presented in Section 1.2.

1.2 DLVO Theory Overview

Colloidal processing of ceramics in particular has been in practice for thousands of years, essentially starting with hand-formed pottery. Since then, advances have been made including technologies such as gel casting and extrusion that are common in ceramic forming today. In recent years, the desire for ceramics optimized to specific engineering applications has led to fundamental scientific research in this area [2], [3], [12], [25]–[27].

This work has led to the evolution of many methods of controlling the mechanical and fluid properties of colloidal ceramics, with stabilization control through electrostatic (DLVO), steric (polymeric), and structural (non-adsorbed species) effects, or any combination of these. The latter two, steric and structural stabilization, introduce a relatively enormous amount of impurities into the system, which must be removed if the final product is intended to be near full density after sintering and have properties approaching those of a bulk engineering ceramic [5].

Steric and structural stabilization techniques have been investigated thoroughly, and are used in a wide variety of additive manufacturing applications [3], [9], [28]–[32]. To achieve a ceramic part whose properties are not compromised by binder material or residual pores, parts made by these methods require complete removal of the binder and densification. The binder removal step usually occurs over a matter of hours to days, and typically a furnace and the power that comes with operating it. Direct coagulation, an electrostatic method, leaves behind little to no residual pores or material, and occurs on the scale of minutes.

From 1939 to 1948, a series of papers by authors Boris **D**erjaguin, Lev **L**andau, Evert **V**erwey, and Jan **O**verbeek were published, outlining what is now commonly known as DLVO theory. This work characterizes the fundamentals of idealized colloid interactions and stability. The theory extends to general interactions between interfaces including deposition. DLVO theory covers a range of possible scenarios including interactions between identical interfaces (symmetric system with homoaggregation), dissimilar interfaces (asymmetric system) and aggregation of dissimilar particles (heteroaggregation).

An idealized metal oxide surface with electrostatic double layer is shown in Figure 8 [33]. The Debye length is shown by a border between the structured arrangement of adsorbed charged particles and the random normal water structure. Also in Figure 8, the inner and outer Helmholz planes are illustrated, differentiating between in initial monolayer of specifically adsorbed ions, and the nonspecifically adsorbed screening layer of opposite polarity. The region beyond this and up to the Debye length is considered the diffuse plane. According to the Bockris-Devanthan-Müller (BDM) model, polar solvent molecules (H_2O) will also arrange themselves in these regions such that each side of the dipole is towards the interface of opposite charge [34].

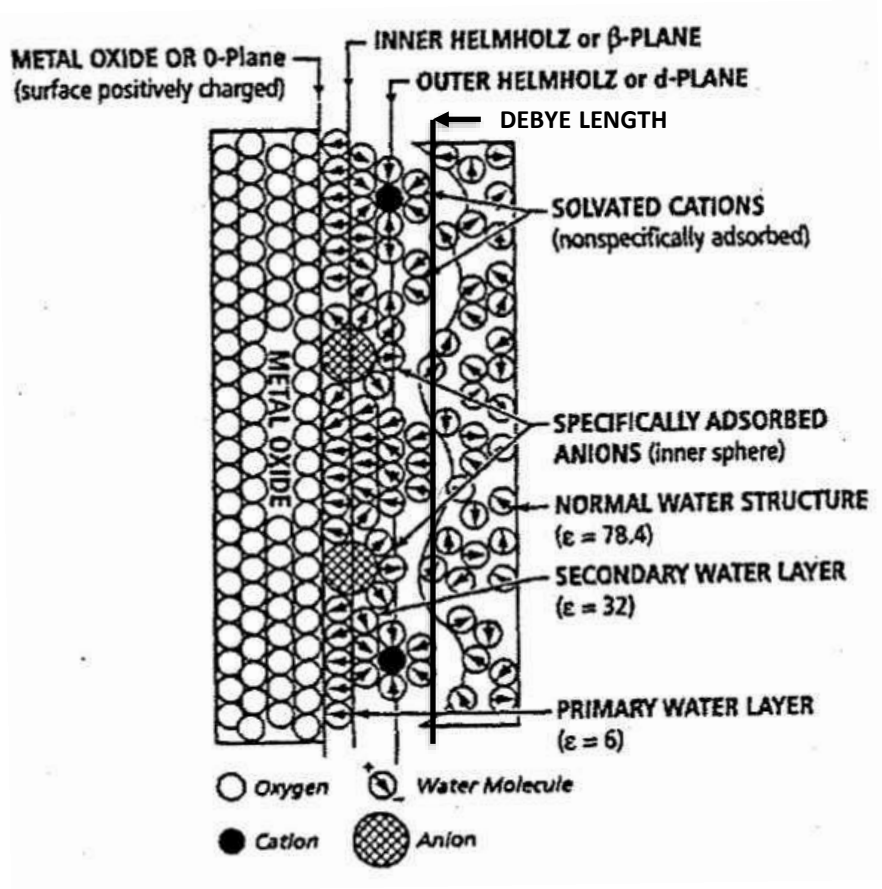

Figure 8: EDL on a metal oxide surface [33]

DLVO theory focuses on the balance of the electrostatic double layer (EDL) force and Van der Waals (VdW) force between particles. EDL force is always repulsive in the case of a symmetric system, is strong at larger distances, and is very strongly dependent on electrolyte concentration and ionic strength [35]. VdW force is affected by particle spacing, such that, as particles become very close, VdW force attracts particles most strongly.

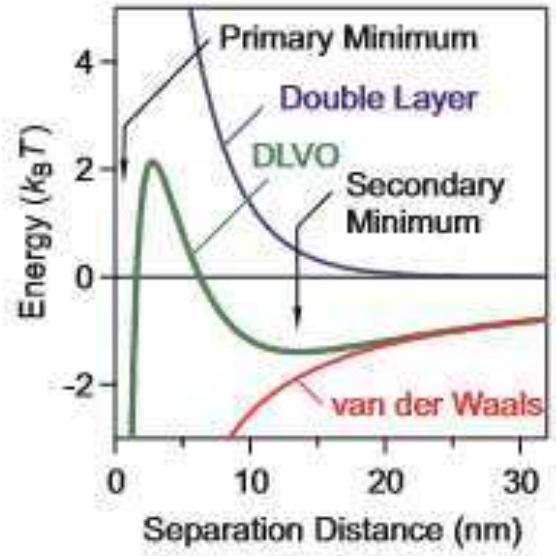

Figure 9: EDL and VdW interaction energy [36]

As shown in Figure 9 [36], DLVO theory describes an energy balance between the two forces. In this theory, there is an energy barrier that must be overcome for particles to make physical contact under extremely attractive VdW forces. The maximum repulsive force occurs approximately at the Debye length (κ^{-1}). This is the distance from the particle surface to where the surrounding cloud of ions acts as a soft static surface attached to the particle, rather than moving freely as if in a liquid. If the EDL repulsion is great enough, colloids will remain stable in suspension, at a separation distance greater than 2 κ^{-1}. If the EDL force is not sufficient, the random motion of particles may provide collisions with enough energy to overcome this barrier and coagulation will occur. EDL force can be

minimized by increasing electrolyte concentration and lowering surface charge density. In either case, a homogenous and stable suspension can be forced to coagulate, forming networks of different density and at a different rate, depending on the degree to which these properties are changed. In general, coagulation methods are useful because particle packing is enhanced, allowing for higher vol% slurries and higher green/sintered densities due to short range repulsive (lubricating) force from EDL and long range attractive force from VdW [37]. DLVO theory is useful in predicting characteristics of slurries, giving insight toward avenues of improvement.

1.3 Sintering Theory Overview

Sintering is commonly defined as the transformation of many particles into a single mass through densification and diffusion processes, under elevated temperature and/or pressure, and without liquefaction. Material transport in sintering occurs in a variety of mechanisms, due to a plethora of driving forces. The most prevalent driving force for sintering is the decreasing of overall internal energy to reach an equilibrium state by reducing surface energy [38]. Aside from this, the other driving forces such as electrical potential and pressure gradients may be present if Joule heating (self heating through electrical resistivity) and/or pressure assisted sintering are used. In pressureless sintering without applied electrical fields, the types of mass transport are surface diffusion, evaporation/condensation, viscous flow, and volume diffusion [39]. In the presence of an applied field or an axial load, with consideration to heating rates, mass transport mechanisms such as electromigration, electrotransport, polarization, and thermodiffusion become significant [40]. Pertaining to the scope of this research, the applicable sintering

theory pertains mostly to “free”, or pressureless, sintering without applied electric fields. In most sintering processes, diffusion is the chief method of mass transport. Sintering by diffusion can be predicted by the Arrhenius temperature relation,

$$\frac{N}{N_0} = exp(-\frac{Q}{RT})$$

Equation 2: Arrhenius Relationship

where $N_0$is the original number of atoms or vacancies in the given area, $N$is the current number of atoms or vacancies, $Q$is the activation energy of the atoms, R is the gas constant, and T is the absolute temperature.

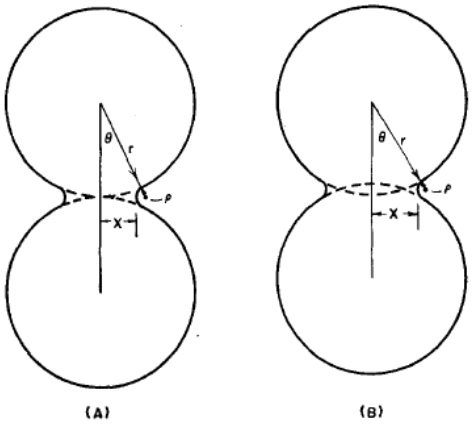

Figure 10: a) Surface diffusion causing neck formation without densification. b) Volume diffusion leading to neck formation and densification [1]

The interparticle diffusion of atoms leads to the development of necks between the theoretically spherical particles of the green part. This can occur in two ways, depending on whether surface diffusion or volume diffusion are dominant, as shown in Figure 10. Surfaces are naturally high-energy areas, as the lattice structure is very frequently disturbed. Due to this, diffusion at surfaces can occur at much lower temperatures than in

the bulk material. Grain boundaries also present high energy, disordered regions, and contribute to diffusion similarly. Typically, surface and grain boundary diffusion are the dominant forms of mass transport from ~0.25-0.5T_m, where T_m is the melting temperature of the material. Beyond 0.5T_m, volume diffusion has the most significant contribution.

Diffusion is a consequence of a nonequilibrium state of energy with regard to interatomic interactions. Diffusion will occur continuously until the equilibrium energy state is reached. Geometrically, a curved surface has a chemical potential greater than a flat surface, and the energy difference is inversely proportional to the particle's radius of curvature [1]. In other words, the smaller the particle, the higher the energy gradient that drives a transformation to a particle with a larger radius of curvature. This can be expressed many ways, but the most applicable is through the relation to intrinsic stress. The intrinsic stress state of a material or grain can be approximated by the Laplace equation,

$$\sigma_{Laplace} = \frac{2\gamma_{sv}}{R}$$

Equation 3: Laplace Stress

where $\sigma_{Laplace}$ is the stress, γ_{sv} is the surface energy of the particle, and R is the radius of the particle. For a material that is not fully dense, as in Figure 11, the Raj stress equation provides a more general approximation that includes pores between grains in the material,

$$\sigma_{Raj} = \frac{2\gamma_{ss}}{D} + \frac{4\gamma_{sv}}{D_p}$$

Equation 4: Raj Stress

where σ_{Raj} is the stress, γ_{sv} is the surface energy of the particle, γ_{ss} is the interfacial surface

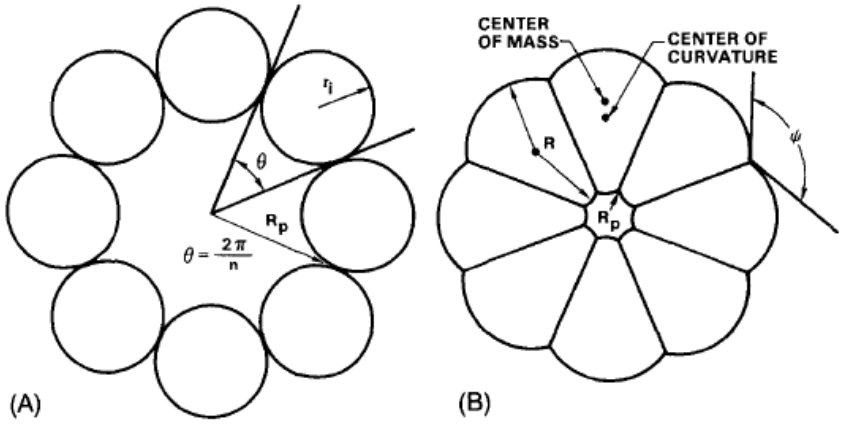

Figure 11: Rings of particles with coordination number n. a) initial condition, b) nonzero contact angle Ψ, initial particle radius R, pore radius Rp, and coordination angle θ [1]

energy, $D$is the diameter of the particle, and $D_p$is the diameter of the pore.

When surface diffusion and evaporation/condensation are the main contributors to the sintering process, no shrinkage of the compact occurs. However, when viscous flow or volume diffusion are the major forms of mass transport, the volume of the compact will shrink during sintering as the particle centers approach each other. In the case of viscous flow, the volume change can be approximated with the Kingery and Berg equation,

$$\frac{\Delta V}{V_0} = \frac{-27n\gamma^2 t^2}{16r^2\eta^2}$$

Equation 5: Kingery and Berg Equation

and in the case of volume diffusion, a similar equation can be used,

$$\frac{\Delta V}{V_0} = \frac{-3n}{8}\left[\frac{80\gamma a^3 D_v}{r^3 kT}\right]^{\frac{4}{5}} t^{\frac{4}{5}}$$

Equation 6: Modified Kingery and Berg Equation

where ΔV is the volume change, V_0 is the original volume, n is the number of contacts per sphere, γ is the surface energy, t is time, r is the radius of the particle, η is viscosity, a is the

atomic radius, D_v is the self diffusion coefficient,k is the Boltzmann constant, and T is the absolute temperature. As can be seen in the above figures, to sinter to full density requires a relatively high green density (typically above 50%) in order to avoid pores that are too large to close completely.

Sintering is traditionally broken into three stages describing discrete phenomena and material characteristics in each stage. There is an initial stage, an intermediate, and a final stage. The material begins as a loose powder before it is sintered. As soon as the temperature is sufficiently high, the initial stage of sintering begins, and is characterized by an open pore structure and high porosity. This is followed by the intermediate stage in which the porosity is reduced by significant interparticle neck growth, grain growth, and pore shrinkage. The final stage can be recognized by significant grain growth and closed, spherical pores, with the potential to reduce porosity to zero if the sample is sintered to full density [1].

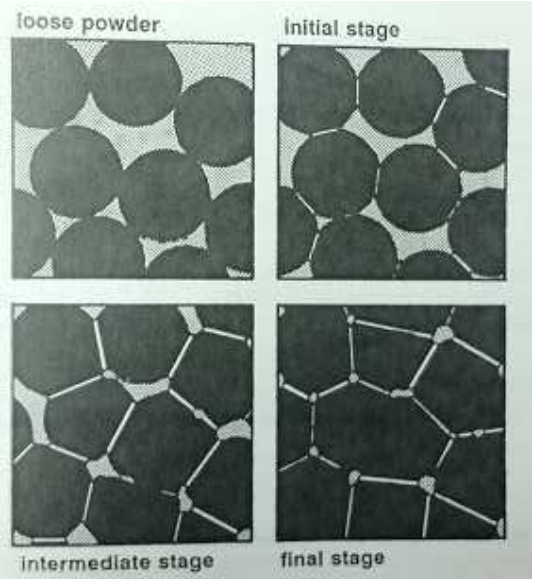

Figure 12: The stages of sintering, starting top left, ending bottom right [1]

1.4 Thesis Outline

With the background information in the previous sections, the remainder of this work is continued with minimal discussion of these fundamentals. Chapter 2 discusses the three suspension types initially investigated and the materials involved; followed by mixing, printing, sintering, microscopy, and mechanical and fluid properties test procedures and equipment used. The results of the experiments and observations are presented and discussed in Chapter 3. This begins with the creation of a high solids content slurry, and then the capability and suitability of each of the three suspension types to printing and sintering. Next is the preliminary optimization of sintering schedules and the chapter is concluded with an in-depth discussion of the direct coagulation printing process and parts created by it. A comprehensive conclusion and proposals for future work are presented in the final pages, in Chapter 4.

References

[1] R. M. German, *Sintering Theory and Practice*. 1996.

[2] J. A. Lewis, "Colloidal Processing of Ceramics," *J. Am. Ceram. Soc.*, vol. 83, no. 10, pp. 2341–2359, Oct. 2000.

[3] G. V. Franks, C. Tallon, A. R. Studart, M. L. Sesso, and S. Leo, "Colloidal processing: enabling complex shaped ceramics with unique multiscale structures," *J. Am. Ceram. Soc.*, vol. 100, no. 2, pp. 458–490, Feb. 2017.

[4] N. Travitzky *et al.*, "Additive Manufacturing of Ceramic-Based Materials," *Adv. Eng. Mater.*, vol. 16, no. 6, pp. 729–754, Jun. 2014.

[5] M. N. Rahaman, *Ceramic Processing and Sintering*, vol. Second Edition. Marcel Decker, Inc., 1995.

[6] T. Mühler, C. M. Gomes, J. Heinrich, and J. Günster, "Slurry-Based Additive Manufacturing of Ceramics," *Int. J. Appl. Ceram. Technol.*, vol. 12, no. 1, pp. 18–25, Jan. 2015.

[7] K. V. Wong and A. Hernandez, "A Review of Additive Manufacturing," *International Scholarly Research Notices*, 2012. [Online]. Available: https://www.hindawi.com/journals/isrn/2012/208760/.

[8] D. Tan *et al.*, "Reduction in feature size of two-photon polymerization using SCR500," *Appl. Phys. Lett.*, vol. 90, no. 7, p. 071106, Feb. 2007.

[9] U. Scheithauer, E. Schwarzer, A. Haertel, H. J. Richter, T. Moritz, and A. Michaelis, "Processing of thermoplastic suspensions for Additive Manufacturing of Ceramic- and Metal-Ceramic-Composites by Thermoplastic 3D-Printing (T3DP)," *Addit. Manuf. Strateg. Technol. Adv. Ceram. Ceram. Trans.*, vol. 258, pp. 19–28.

[10] U. Scheithauer, E. Schwarzer, T. Moritz, and A. Michaelis, "Additive Manufacturing of Ceramic Heat Exchanger: Opportunities and Limits of the Lithography-Based Ceramic Manufacturing (LCM)," *J. Mater. Eng. Perform.*, pp. 1–7, Aug. 2017.

[11] S. Zhao, W. Xiao, M. N. Rahaman, D. O'Brien, J. W. Seitz-Sampson, and B. Sonny Bal, "Robocasting of silicon nitride with controllable shape and architecture for biomedical applications," *Int. J. Appl. Ceram. Technol.*, vol. 14, no. 2, pp. 117–127, Mar. 2017.

[12] J. T. Muth, P. G. Dixon, L. Woish, L. J. Gibson, and J. A. Lewis, "Architected cellular ceramics with tailored stiffness via direct foam writing," *Proc. Natl. Acad. Sci.*, vol. 114, no. 8, pp. 1832–1837, Feb. 2017.

[13] D. Prawel, "Advanced/Additive Manufacturing Engineering: Principles of Extrusion," Colorado State University, 2017.

[14] J. Gonzalez-Gutierrezz, G. Stringari Beulke, and I. Emri, "Powder Injection Molding of Metal and Ceramic Parts," in *Some Critical Issues for Injection Molding*, Intech, 2012.

[15] M. Mekhail, J. Daoud, G. Almazan, and M. Tabrizian, "Rapid, Guanosine 5'-Diphosphate-Induced, Gelation of Chitosan Sponges as Novel Injectable Scaffolds for Soft Tissue Engineering and Drug Delivery Applications," *Adv. Healthc. Mater.*, vol. 2, no. 8, pp. 1126–1130, Aug. 2013.

[16] K. Prabhakaran, S. Raghunath, A. Melkeri, N. M. Gokhale, and S. C. Sharma, "Novel Coagulation Method for Direct Coagulation Casting of Aqueous Alumina Slurries Prepared Using a Poly(Acrylate) Dispersant," *J. Am. Ceram. Soc.*, vol. 91, no. 2, pp. 615–619, Feb. 2008.

[17] R. Greenwood and K. Kendall, "Selection of Suitable Dispersants for Aqueous Suspensions of Zirconia and Titania Powders using Acoustophoresis," *J. Eur. Ceram. Soc.*, vol. 19, no. 4, pp. 479–488, Apr. 1999.
[18] S. Dhara and P. Bhargava, "A Simple Direct Casting Route to Ceramic Foams," *J. Am. Ceram. Soc.*, vol. 86, no. 10, pp. 1645–1650, Oct. 2003.
[19] S. Dhara and P. Bhargava, "Influence of Nature and Amount of Dispersant on Rheology of Aged Aqueous Alumina Gelcasting Slurries," *J. Am. Ceram. Soc.*, vol. 88, no. 3, pp. 547–552, Mar. 2005.
[20] J.-H. Jean and H.-R. Wang, "Effects of Solids Loading, pH, and Polyelectrolyte Addition on the Stabilization of Concentrated Aqueous BaTiO3 Suspensions," *J. Am. Ceram. Soc.*, vol. 83, no. 2, pp. 277–280, Feb. 2000.
[21] D. J. Shanefield, *Organic Additives and Ceramic Processing: With Applications in Powder Metallurgy, Ink, and Paint*. Springer Science & Business Media, 2013.
[22] J. He *et al.*, "Dispersion of nano-sized yttria powder using triammonium citrate dispersant for the fabrication of transparent ceramics," *Ceram. Int.*, vol. 8, no. 42, pp. 9737–9743, 2016.
[23] J. Xu, Y. Zhang, Y. Qu, F. Qi, X. Zhang, and J. Yang, "Direct Coagulation Casting of Alumina Suspension from Calcium Citrate Assisted by pH Shift," *J. Am. Ceram. Soc.*, vol. 97, no. 4, pp. 1048–1053, Apr. 2014.
[24] E. E. Luther, J. A. Yanez, G. V. Franks, F. F. Lange, and D. S. Pearson, "Effect of Ammonium Citrate on the Rheology and Particle Packing of Alumina Slurries," *J. Am. Ceram. Soc.*, vol. 78, no. 6, pp. 1495–1500, Jun. 1995.
[25] Y. De Hazan, J. Heinecke, A. Weber, and T. Graule, "High solids loading ceramic colloidal dispersions in UV curable media via comb-polyelectrolyte surfactants," *J. Colloid Interface Sci.*, vol. 337, no. 1, pp. 66–74, Sep. 2009.
[26] J. A. Lewis, J. E. Smay, J. Stuecker, and J. Cesarano, "Direct Ink Writing of Three-Dimensional Ceramic Structures," *J. Am. Ceram. Soc.*, vol. 89, no. 12, pp. 3599–3609, Dec. 2006.
[27] Q. Li and J. a. Lewis, "Nanoparticle Inks for Directed Assembly of Three-Dimensional Periodic Structures," *Adv. Mater.*, vol. 15, no. 19, pp. 1639–1643, Oct. 2003.
[28] U. Scheithauer, E. Schwarzer, H.-J. Richter, and T. Moritz, "Thermoplastic 3D Printing—An Additive Manufacturing Method for Producing Dense Ceramics," *Int. J. Appl. Ceram. Technol.*, vol. 12, no. 1, pp. 26–31, Jan. 2015.
[29] X. Yan and P. Gu, "A review of rapid prototyping technologies and systems," *Comput.-Aided Des.*, vol. 28, no. 4, pp. 307–318, Apr. 1996.
[30] L. García-Gancedo *et al.*, "Application of gel-casting to the fabrication of 1–3 piezoelectric ceramic–polymer composites for high-frequency ultrasound devices," *J. Micromechanics Microengineering*, vol. 22, no. 12, p. 125001, 2012.
[31] K. Stuffle, A. Mulligan, J. Lombardi, P. Calvert, and B. Fabes, "Solid Freebody Forming of Ceramics from Polymerizable Slurry," *MRS Online Proc. Libr. Arch.*, vol. 346, Jan. 1994.
[32] R. Garg, R. K. Prud'homme, I. A. Aksay, V. F. Janas, K. S. Tenhuisen, and S. T. Huxel, "Controlled architecture ceramic composites by stereolithography," US6283997 B1, 04-Sep-2001.
[33] D. J. Wesolowski, D. A. Palmer, P. Benezeth, and L. M. Anovitz, "Surface Charge and Ion Adsorption on Metal Oxides to 290 C." Oak Ridge National Laboratory.

[34] J. O. Bockris, M. a. V. Devanathan, and K. Müller, “On the structure of charged interfaces,” *Proc R Soc Lond A*, vol. 274, no. 1356, pp. 55–79, Jun. 1963.
[35] M. A. Brown *et al.*, “Determination of Surface Potential and Electrical Double-Layer Structure at the Aqueous Electrolyte-Nanoparticle Interface,” *Phys. Rev. X*, vol. 6, no. 011007, 2016.
[36] G. Trefalt and M. Borkovec, *Overview of DLVO Theory*. 2015.
[37] B. V. Velamakanni, J. C. Chang, F. F. Lange, and D. S. Pearson, “New method for efficient colloidal particle packing via modulation of repulsive lubricating hydration forces,” *Langmuir*, vol. 6, no. 7, pp. 1323–1325, 1990.
[38] B. J. Kellett and F. F. Lange, “Thermodynamics of Densification: I, Sintering of Simple Particle Arrays, Equilibrium Configurations, Pore Stability, and Shrinkage,” *J. Am. Ceram. Soc.*, vol. 72, no. 5, pp. 725–734, May 1989.
[39] W. D. Kingery and M. Berg, “Study of the Initial Stages of Sintering Solids by Viscous Flow, Evaporation-Condensation, and Self-Diffusion,” *J. Appl. Phys.*, vol. 26, no. 10, pp. 1205–1212, Oct. 1955.
[40] U. Anselmi-Tamburini, G. Spinolo, F. Maglia, I. Tredici, T. B. Holland, and A. K. Mukherjee, “Field Assisted Sintering Mechanisms,” in *Sintering*, Springer, Berlin, Heidelberg, 2012, pp. 159–193.

2 Experimental Methods, Measurements, and Instruments

While many methods were employed, extrusion based ceramic additive manufacturing generally adheres to a process flow common to all techniques. This process flow involves three main operations, slurry preparation, printing, and sintering, and is illustrated in Figure 13. The details of each process varied significantly between methods, but the end result accomplished the same goal. Before, during, and after these processes, measurements and observations were made to characterize both the material system and the process itself. These included SEM for initial powder characterization, viscosity and zeta potential testing to understand fluid and colloidal properties, and hardness and flexural testing to obtain mechanical properties.

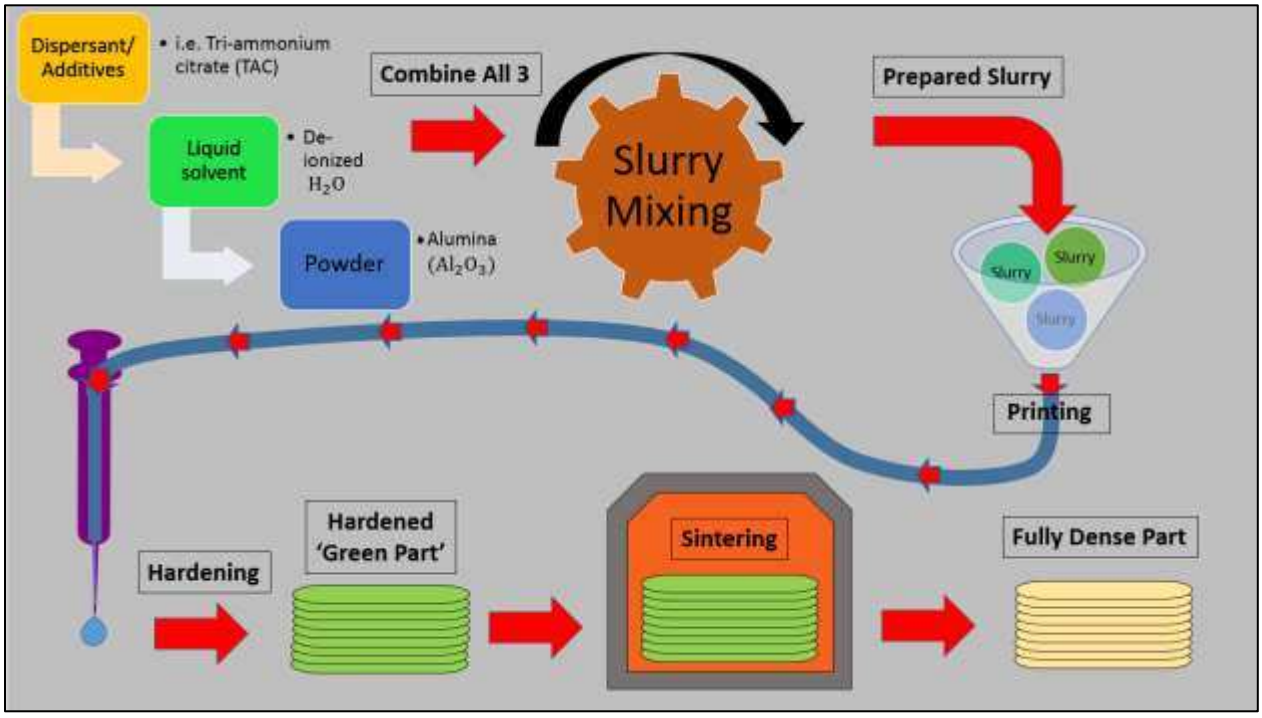

Figure 13: Experimental Process Flow

2.1 Powder Characterization

Characterization of powders in the 'as-received' state is necessary prior to experimentation to validate manufacturer's specifications and quantify unknown properties. Two different types of α-alumina (Al_2O_3) were used in printing experiments; one being more expensive and of very high quality (*99.9999%, 100 nm avg. dia., TM-DAR, Taimei Chemicals Co, Japan*), and another being more affordable, lower purity, and having larger grain size (*99.0%, 150 nm avg. dia., Skyspring Nanomaterials, USA*).

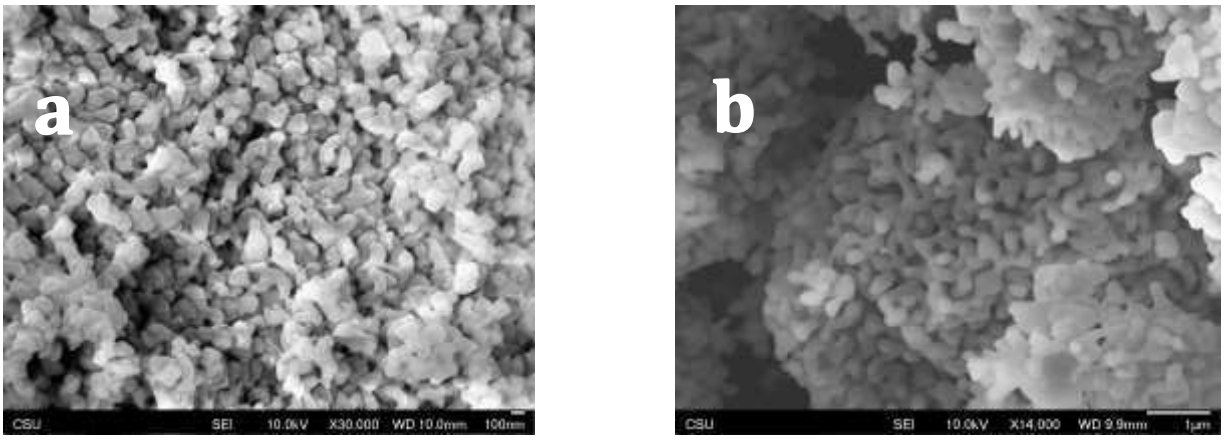

Figure 14: a) Taimei Powder, b) Skyspring Powder

The SEM images in Figure 14 were taken to validate grain size and morphology of each powder. Grain size is a very important factor in colloidal science because it determines the ratio of surface area to mass of powder. Through this, either the electrical forces at the surface or gravitational forces due to mass will dominate, determining the ability of particles to be suspended indefinitely. Grain size is also impactful in sintering, as nanoparticles can have significantly reduced energy demands to produce fully dense parts as compared to conventional micron-scale particles or larger. To validate many assumptions in sintering and DLVO theory, it is necessary to know morphology, or general

shape of a grain. Nearly all sintering and colloid theory is based on the assumption of spherical particles.

2.2 Preparation of Various Slurries

In the initial stages of this research, three candidate material systems were investigated. The main mechanism of each system was fundamentally different; a bio-polymer gel, a functionalized polymer binder, and a directly coagulating suspension. Each of these, and any particular intricacies in their preparation, are described in the sections below.

2.2.1 Chitosan (pronounced kite-o-san)

The first method investigated in this research was based on a rapidly crosslinking bio-polymer system involving chitosan and guanosine 5 diphosphate (GDP) as crosslinking agent. For this method, chitosan (740063 High Purity Chitosan, M_v 60,000-120,000, Sigma Aldrich, USA) was dissolved at either 3 or 6 mg/mL in a 0.06M solution of hydrochloric or acetic acid. Alumina powder was then added to this solution. Due to the fact that the powders remained in suspension and did not show aggregation or clumping, it was assumed to be sterically stabilized. After powder was added, a solution of GDP (G7127, 96% purity, Sigma Aldrich, USA) at 100mg/mL in DI water was made and added to the chitosan and powder solution at 15 vol%. This was then stirred by hand to facilitate rapid and homogenous crosslinking. This reaction occurred on the order of seconds, and the stabilization method was assumed to have transitioned to a structural stabilization. From this point, the parts were already a semi-solid gel, and would need the gel structure removed before or during the sintering process to achieve fully dense ceramic parts.

2.2.2 PVA Binder

To make a sterically stabilized ceramic suspension, Darvan 821-A was added at 0.3 wt% with respect to alumina powder. The slurries were mixed in a ball mill with 50 vol% Al_2O_3, DI water, and Darvan until fully liquid. With a low viscosity, high solids content slurry achieved, the binder polyvinyl alcohol (PVA) was mixed in by ball mill to produce the increase in viscosity to a printable state. This was added at either 19 or 8 vol% with respect to Al_2O_3. After mixing, the slurry was ready to be loaded into a syringe and extruded, then dried and sintered. The temperature of the print bed was adjusted between room temperature and 80°C to produce different drying rates. Burnout of the contaminants occurs during a heating step in the sintering process.

2.2.3 TAC Only

Making a slurry with high solids loading with TAC alone required many iterations and different mixing methods. In general, the process began with dissolution of 0.3-0.5 wt% TAC, with respect to alumina, in DI water. This solution was then added to alumina powder at 40-50 vol% in the required mixing container (varied with each mixing method, discussed in Section 2.3) with the corresponding media. Of critical importance, regardless of the mixing method, the container must be very well sealed to eliminate evaporation of ammonia or water during mixing and any time before printing. It was not until the mixing process was perfected that experimentation with further modification of the slurry by pH adjustment was attempted. The freshly mixed slurry exhibited a pH around 8.5-9.5 and near water viscosity; this was adjusted by addition of 2M HNO_3 to a pH between 4.2-5.2 to produce an extrudable and much more stable gel. During extrusion, print bed temperature could be modified to alter coagulation

characteristics. Once completely coagulated into a hard solid, the parts could be sintered without a binder removal step.

The evolution of the mixing process involved many techniques including hand mixing, a simple magnetic stir bar, a roller mill, a SPEX mill, and a planetary ball mill. Each of these required specific speeds and most required mixing media with a specific ball:powder mass ratio to be successful.

2.3 Slurry Mixing

In an endeavor to develop the most efficient process of mixing a slurry for printing, a variety of mixing techniques were investigated. The preferred mixing method should balance batch size, mixing time, and consistency, with respect to the application. In a simple feasibility test, a small batch size is acceptable, minimum mixing time is preferred, and repeatability can be optimized later. On the other hand, to print a large part as the culmination of an optimization of a slurry, a large batch size is required, mixing time is not important, and the repeatability of the method must be very high to ensure the slurry exhibits the expected extrusion characteristics. In either case, the higher the achievable solids content, the better the mixing method. This is because, as long as the slurry still shows fluid behavior for extrusion, higher solids content leads to a denser green body and less shrinkage. A denser green body provides better sinterability, while less shrinkage helps mitigate warping and cracking during printing and sintering [1], [5]. The various mixing methods and their operation are described in the rest of this section. The results and employment of each technique are discussed in Chapter 3.

2.3.1 Hand Mix and Stir Bar

Mixing by hand was done in either a glass or plastic container, with a stainless-steel spatula. Typically, only very low solids content (<35 vol%) was achievable due to the relatively low amount of kinetic energy involved. The batch size can be scaled to very large (hundreds of milliliters), but containers cannot be sealed. Hand mixing can also be a time-consuming process, and is relatively inconsistent. This method provides easy preliminary results for the mixability and particle suspension characteristics of a material system. During and after mixing, the flow and settling of the slurry can be qualitatively analyzed.

Mixing with a magnetic stir bar in the bottom of a glass or plastic container provides very similar capability to hand mixing, with the added ability to stir at a measured rate, work in a sealed container, and with slightly more energy than by hand. This can provide slightly higher solids content slurries when allowed to run for hours. The batch size is limited by stir bar size, but still relatively large. Consistency is also increased over hand mixing. This can be a good preliminary mixing step for slurries necessitating a sealed container, or an intermediate mixing step for slurries that showed promise with hand mixing.

2.3.2 Mixing/Milling Machines

Three types of industrial mixing machines were used in this research; a roller mill, a high energy ball mill (HEBM), and a planetary ball mill.

The roller mill is a very traditional machine for slurry mixing. The basic principle of operation is to rotate a container on its side at such a rate that the contents remain on the wall due to friction or centrifugal effects until they are nearly at the top, at which point gravity forces them to fall back down. With repetition, a significant amount of energy can be put into mixing, especially if mixing media is added. In this way, agglomerates are

broken up by the impact of media and slurry on the bottom of the container, and mixing naturally occurs through this process as well. This process allows for sealed containers. As the slurry becomes increasingly well-mixed, the viscosity changes, and the optimum rotation speed changes accordingly. This makes the repeatability of the method very low, considering it may need to run overnight, when, without supervision, a change in viscosity may occur without an operator present to adjust speed. This mixing method can accommodate large samples, but requires very long mixing times to achieve liquid slurries with high solids content, as it is still relatively low energy. For this research, a basic roller mill (U.S. Stoneware, USA), with plastic jars and 5 mm spherical alumina mixing media was used.

The HEBM operates on an eccentric rotation, with axial movement as well as radial, causing more random and complete mixing. In this research, an 8000M Mixer (Spex Sample Prep, USA) was used, with a stainless-steel mixing jar and 10 mm spherical stainless-steel mixing media. This is a very high energy mixing process, using a 1/3 horsepower motor and spinning at over 1000 cycles per minute, resulting in extremely low mixing times of 2-5 minutes, as compared to hours with other mixers. However, the machine is only designed for very small samples, allowing for only about 7.5 mL of slurry to be made at one time. The consistency of this method is very high.

The final mixing machine to be mentioned is the planetary ball mill. This operates by rotating a base plate, with the media in jars on separate rotating platforms that spin counter to the direction of the base plate, reminiscent of the popular 'tea cup' ride seen at carnivals. The counter-rotation of the plate beneath the mixing jars causes the media and slurry to be forced from one wall to another, instead of constantly circling the outside of

the jar, as shown in Figure 15. This mixing method allows for relatively large batch production (~100 mL), but can require hours to days to mix a large amount of slurry. When mixing only small amounts, mixing can be done in a matter of a few hours. When working with slurries that are very sensitive to very small quantities of dispersant, such as with TAC, the ability to make a large batch helps mitigate the amount of error involved in measuring such small quantities. This method shows very high consistency, but only when particular care is taken to ensure a good seal in the jars. Due to the long mixing times and heat that builds up in the jars from the constant friction, a bad seal may allow the escape of enough volatile constituents to render the slurry unmixable, resulting in a hard, dry clump instead of liquid suspension. The three mixing machines are shown in Figure 16.

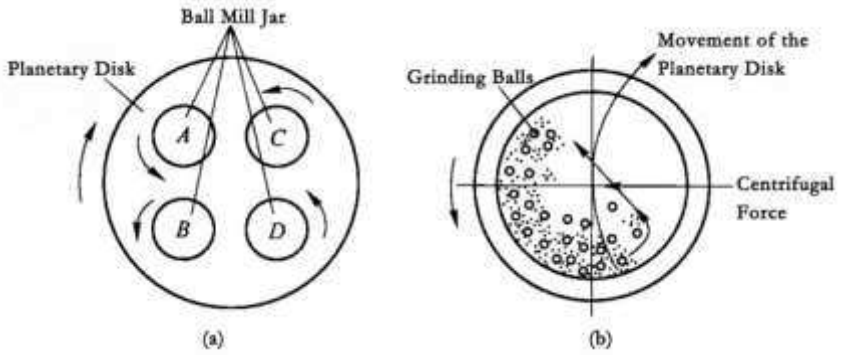

Figure 15: Diagram of a planetary ball mill, a) overview of planetary disk, b)cross section of a jar, showing force created by planetary disk

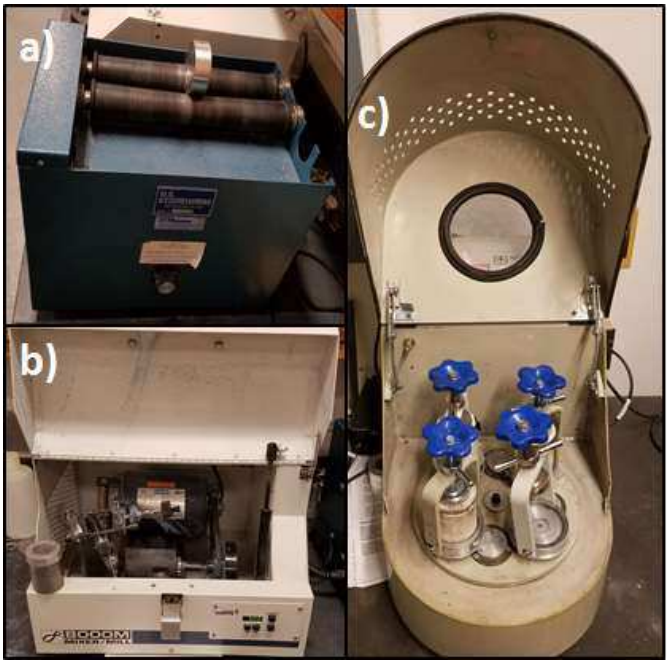

Figure 16: Mixing machines. a) Roller mill b) SPEX high energy ball mill c) Planetary ball mill

Once a slurry is mixed via the chosen method and the desired fluid properties are achieved, the material is ready for printing.

2.4 Printing

As mentioned earlier, there are a multitude of printing systems, with many requiring completely different hardware. The direct coagulation system was designed with versatility and ease of implementation in mind. The relatively straightforward process of extrusion in ambient conditions has requirements that are fulfilled by most polymer extrusion printers, and an easy conversion can normally be done to enable DCP. Although, similar to the extrusion process, when environmental conditions are not held relatively constant, it can be difficult to optimize printing parameters. Essentially, printing involves first getting a suitable printer, then managing the three different processes of extrusion, toolpath generation, and curing.

2.4.1 The Printer

The scope of this research focuses on material and process development, so the decision was made to avoid time-intensive hardware development of a custom 3D printer. Hence, a Lulzbot® Mini was acquired and modified with a syringe pump style extruder. To further minimize hardware development, the modification was done using the open-source CAD files for "Universal Paste Extruder for 3D Printers" from user RichRap on the CAD sharing website thingiverse.com. The parts for this were printed with ABS filament on the Mini, making use of its original function as a heat-extrusion thermoplastic printer. Once assembled, the syringe pump was mounted in place of the thermoplastic extruder, the resulting difference in gear reduction was calculated, and flow rates were adjusted accordingly in the software. To reduce environmental variability, the printer was placed in an enclosure, as seen in Figure 17.

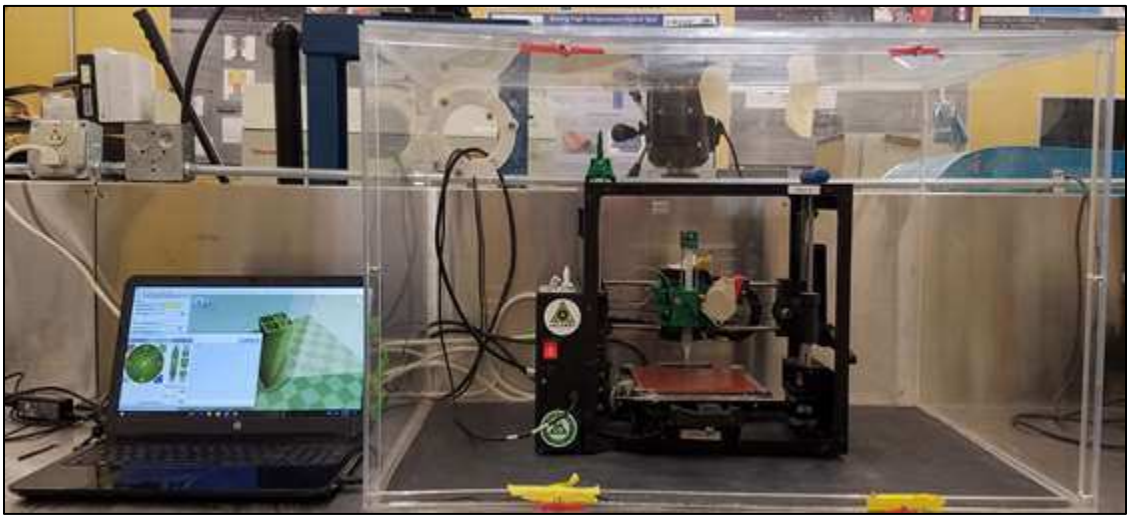

Figure 17: Lulzbot Mini printer modified for slurry extrusion

After initial experimentation, it was found that the extrusion pressure required for high viscosity slurries was more than the ABS gears could handle, leading to frequent clogging of the syringe nozzle and eventual failure of the ABS transmission. As a remedy, an aluminum transmission was designed and machined in-house. Once the metal transmission

was installed, significantly higher extrusion pressures were achieved, allowing testing with much higher viscosity slurries. The original and metal gears can be seen in Figure 18.

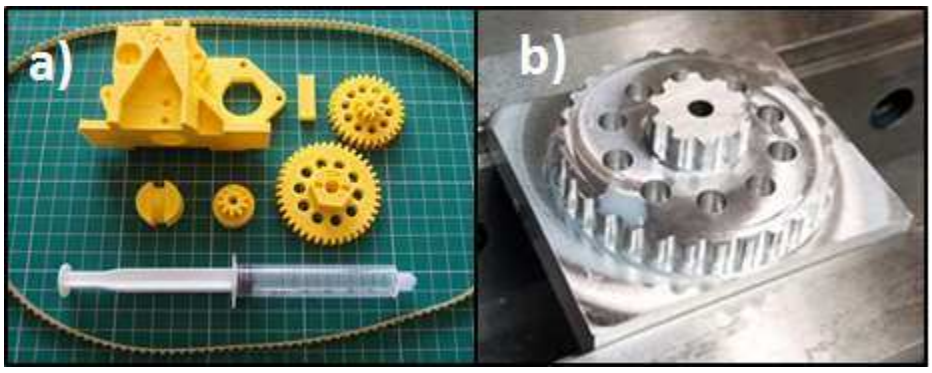

Figure 18: a) Printed syringe pump extruder with plastic gears, b) custom aluminum gears in the process of being machined

2.4.2 Syringe Extrusion

With a slurry capable of coagulating in a predictable and repeatable manner, extrusion methods could be tested. For the purposes of this research, successful extrusion included being able to produce parts with consistent, predictable geometry and the ability to create complex geometries. Complex geometry is defined in this research as something that would be either inhibitively difficult or simply impossible without the use of additive manufacturing. Experiments testing extrusion were performed using a syringe with a needle tip having a nozzle diameter of 0.6 mm. Slurry was extruded onto a glass or epoxy coated print bed held at temperatures. For these samples, the degree of coagulation was determined by the samples' resistance to deformation. When the sample no longer deformed during attempts to remove it from the print bed, it was considered to be solid and completely coagulated.

2.4.3 Toolpath Programming

In order to make the desired geometry, a 3D printer must be programmed with g-code describing the geometry and printing parameters to be used. To accomplish this, there

are a few open-source software packages called “slicers”, capable of generating g-code from CAD geometries saved as stereolithography (.stl) files. Due to the fact that the printer used in this research was a Lulzbot printer, the slicer used was the Lulzbot-specific version of Cura. This slicer allows for control of many of the printing parameters, however, modification of individual toolpaths can be very difficult and time consuming. For this reason, the default toolpaths generated for any specified geometry or infill pattern were not modified. This choice was made for expediency, and it should be noted that custom toolpaths designed for DCP would likely result in higher quality parts.

2.4.4 Curing

Once solid, many methods require an additional period of time for parts to cure. This can involve the completion of a chemical reaction, or simply evaporation of adsorbed water, which can take significantly longer than the solidification process. Curing was done in atmosphere and inside of an enclosure to regulate and limit air flow which could introduce rapid changes in humidity and temperature. Many times, samples were printed onto a removable substrate and left to cure on the substrate to minimize risk of damaging the part with premature stress during removal from the print bed itself. Green parts were determined to be fully cured when they no longer exhibited mass loss over time (likely the slow evaporation of adsorbed water), even if the coagulation was complete and parts could not be deformed without breaking.

2.5 Sintering

Sintering was performed in atmosphere, under pressureless, or ‘free’, sintering conditions. This is a very traditional sintering method, requiring no specialty tooling,

fixtures, or instruments, beyond a high-temperature furnace. To achieve full density by this method is evidence of a green part with a very favorable structure for sintering. Free sintering requires very low total energy input compared to other methods, as it does not involve pressurization or generation of electric fields in addition to simple resistive heating. For this research, all sintering was performed in a high temperature box furnace (Model 4610, Thermolyne, USA).

Generally, when trying to create fully dense materials, bulk, or volume, diffusion is the preferred dominant form of mass transport, generating the most densification. As mentioned in Section 1.3, volume diffusion dominates after the temperature surpasses approximately half the material's melting temperature. For this reason, the sintering schedules in this research consist of a fast heating ramp to a temperature near 0.75 T_m and held there for a period of time, then cooled relatively slowly to avoid part failure by thermal shock. Sintering parameters were varied in response to experimental results until a reliable procedure for producing fully dense parts was developed.

2.6 Mechanical Testing

For ceramics to be used reliably as structural engineering materials, an understanding of the mechanical properties is necessary. A comparison of these properties with published values gives insight into quality and potential applications. In the field of ceramics, hardness and elastic modulus are two of the most commonly reported values. To measure these, the samples must be prepared such that the assumptions for the test method are satisfied, such as flatness and perpendicularity of sides. Once specimens have

the ideal geometry, they can be analyzed and compared to other studies which used similar testing methods.

2.6.1 Surface Preparation

Surfaces of printed and sintered parts were polished prior to mechanical testing to ensure a flat and ideal testing surface. This was accomplished by mounting samples to a flatting tool and abrading with either SiC or diamond abrasive pads and suspensions. Mechanical polishing was performed with media beginning at 240 grit, and ending with media as small as 1 μm. For many samples, it was necessary to create a perfectly rectangular beam, so four polished sides were made, and perpendicularity was checked.

2.6.2 Hardness Testing

Hardness values were determined according to the Vickers Microhardness (HV) scale. This method has been widely used on ceramics. The tests were performed on flat, polished samples, with a diamond pyramid indenter, a 9.8 N load, and a 15 second hold time, according to ASTM E384-16 on an HV1000Z Microhardness Tester (Pace Technologies, USA). Due to the inherent brittleness of ceramics, samples are prone to spalling during indentation. Because the spalling dissipates some of the energy, the degree of indentation can be reduced, indicating a failure of the material that can significantly skew the hardness measurement. To ensure accurate hardness measurements, all indents were inspected for spalling under an optical microscope and discarded from data sets if spalling had occurred.

2.6.3 Four-Point Bend Testing

Four-point bend testing was done to evaluate both flexural modulus and flexural strength. When testing ceramics, it must be kept in mind that inherent flaws such as pores

are statistically unavoidable. These flaws are often distributed randomly throughout the ceramic. Four-point bending generates a constant load along most of the beam, so if there is a flaw anywhere in the beam, failure will occur there before the ultimate load for a flawless section is achieved. This differs from three-point bending, in which the load is always highest in the center of the beam, so if flaws are not directly under the loading point, they may not lead to failure before the bulk material reaches its ultimate load. For this reason, four-point bending gives a more comprehensive understanding of the material properties when inherent flaws must be accounted for.

Four-point bend testing was performed according to ASTM C1161 on an Instron testing machine (Model 8501, Instron, USA) with a crosshead speed of 0.127 mm/min.

2.7 Fluid Properties Characterization

As important as the mechanical properties are to the end use of the parts, the fluid properties are just as critical to extrusion and shaping of parts. While all the approaches involved significant changes in fluid properties during printing, the measured values represent the suspension in a freshly mixed state, before being loaded into the syringe for extrusion, unless otherwise noted.

2.7.1 Zeta Potential

Dielectric materials that are submerged in aqueous electrolyte solutions develop an electric field that surrounds them. This field can be described by its strength at various positions, however very few of these are easily measured. One method of characterization of this field is by charge at the edge of the diffuse second layer, or the slipping plane, known as the zeta potential. This represents the electric potential between bulk solvent and the

charged particles adsorbed to the colloid surface. For this research, the zeta potential was found using Dynamic Light Scattering (DLS).

DLS, also known as photon correlation spectroscopy, is most widely known as a tool for particle size measurement, but zeta potential and rheological properties may also be found in this way. The instrument uses lasers pulsed at the microsecond scale and measures the doppler shift caused by particle motion in an applied electric field. Zeta potential can be determined as a function of this electrophoretic mobility by rearranging the Smulochowski theory [41] as shown in (2).

$$\zeta = \frac{\mu_e \eta}{\varepsilon_r \varepsilon_0}$$

Equation 7: Zeta Potential

ζ is the zeta potential, μ_e is the electrophoretic mobility, η is the solvent viscosity, ε_r is the dielectric constant of the particles, and ε_0 is the permittivity of free space. This method is known as electrophoretic light scattering, as opposed to static light scattering, which is used to determine particle size and molecular weight.

Zeta potential measurements were done using a Malvern Zetasizer Nano ZS (Malvern Instruments, United Kingdom). The machine uses a 633 nm red laser, shining through a transparent cuvette. In testing, cuvettes were filled with suspensions of alumina at 0.5 vol% containing TAC at various concentrations or various pH levels. As mentioned in Chapter 1, zeta potential should be high in magnitude when a suspension is stable, and at low zeta potential, coagulation or settling can occur.

2.7.2 Viscosity

Viscosity was measured using a Viscolead Pro viscometer (Fungilab, Spain). This is a concentric cylinder style viscometer, generating Couette flow. For the viscosity to be calculated by the instrument, three pieces of information must be known, the spindle geometry, the torque on the motor rotating the spindle, and the shear rate of the spindle. For this research, an L4 spindle was used, with a shear rate of 132 s^{-1}. The torque was measured by the instrument, and viscosity was displayed.

2.7.3 pH Measurement

pH is the inverse logarithm of the concentration of H^+, or protons, in a substance, and can be measured by the charge created on a probe in contact with the sample. Some of the material systems that were measured were dynamic, meaning pH changes naturally over time. For these, pH was measured during any pH adjustment, and directly before printing. Tests were done using a handheld pH meter (PH150, Oakton, USA) with a multifunction temperature/pH probe.

2.8 SEM Analysis

Microscopy is essential to understanding the microstructure of materials, and Scanning electron microscopy (SEM) allows for very high magnification and resolution images. SEM requires that a focused beam of electrons bombard the object to be observed, and are emitted to be captured by the detectors. It can be difficult to achieve an ideal image when working with ceramics, which can acquire a strong surface charge due to their inability to conduct the electrons bombarding them. For this reason, it is very helpful to coat the samples with a thin layer of conductive material, such as gold, which is easily sputtered. In order to view the microstructure in true cross section, samples were polished

for observation. SEM was performed using a JSM – 6500F scanning electron microscope (JEOL Inc, USA). Best results were usually acquired with approximately 10 nm of sputtered gold coating and 10kV accelerating voltage.

References

[1] R. M. German, *Sintering Theory and Practice*. 1996.
[5] M. N. Rahaman, *Ceramic Processing and Sintering*, vol. Second Edition. Marcel Decker, Inc., 1995.
[41] M. Smoluchowski, “Contribution à la théorie de l’endosmose électrique et de quelques phénomènes corrélatifs,” *Pisma Mariana Smoluchowskiego*, vol. 1, no. 1, pp. 403–420, 1924.

3 Results and Discussion

In this chapter, experimental findings are presented for an assortment of tests developed to characterize the printing materials and methods used in this research. This begins with the challenge of developing a slurry with adequately high solids content for near-net green part formation. Following that, the search for an appropriate method of particle stabilization and printing is related. Finally, investigations in optimizing printing and sintering parameters for the direct coagulation method are reported. The final section of this chapter consists of a paper written for publication in the peer-reviewed journal *Additive Manufacturing*. Following this, a discussion of the applications and implications of the technology is put forward.

3.1 Investigation of High-Solids Slurry Mixing

Creation of a slurry with appropriately high solids content for sintering to full density was critical to the goals of this work. In general, this requires not only a large amount of energy, but also materials with an amenable difference in surface tension. The latter ensures a more energetically efficient wetting of solid surfaces by the liquid. In lieu of changing the nanopowder, the solvent may be modified with additives that lower the surface tension. As for the amount of energy required to mix, this variable was modified by using the different mixing machines available.

3.1.2 Optimizing the Mixing Process

The roller mill was the first method to which optimization experiments were performed. Eventually, it was found that the roller mill was a very inconsistent and time intensive process. Mixing times ranging from hours to days were observed. As explained in

Chapter 2, mixing in a roller mill requires adjustment of speed to fit the material's viscosity. Variables that were investigated included batch size, rotational speed, and duration at each speed. These varied from 5mL to 50mL samples, from 10 rpm to 80 rpm, and 30 minutes to 8 hours, respectively. A ball:powder mass ratio of 1:1 was used in all testing. Results were inconsistent to the degree that alternative mixing methods were sought out before finishing optimization on the roller mill. With gravity providing a significant portion of the total mixing energy, the roller mill provides the least total kinetic energy of all methods available.

In order to determine if the issues seen in mixing could be overcome with a higher energy method, the SPEX high energy ball mill was used. It was assumed that optimization would be necessary, and a DOE was planned to investigate all possible parameters. Upon the first attempt to mix a 7.5 mL 50 vol% slurry with 0.3 wt% TAC as dispersant, a very homogenous and low viscosity slurry was produced with 4 minutes of mixing. With this result, and the consistency of those that followed, it was determined that the complications seen on the roller mill could indeed be overcome with a more energetic process, without needing to perform a DOE. Overall, mixing times in the SPEX mill ranged from 1 to 10 minutes. The ball:powder mass ratio fluctuated with sample size, as only one set of two stainless steel milling balls, weighing 16 grams, were available. This resulted in ratios from about 2:1 to about 0.75:1. The only downside of this method was that it can only accommodate very small samples (up to 10 mL). In anticipation of printing larger parts, larger quantities of slurry were desired. Making batches back to back in the SPEX was impractical, as, immediately on exposure to atmosphere, one batch would begin to

coagulate before another was finished mixing. Hence, a mixing solution capable of larger batch sizes became necessary.

The planetary ball mill provides an intermediate level of kinetic energy, between the high energy ball mill and the roller mill, and can handle batch sizes up to 80 mL. After initial experimentation, results were once again highly inconsistent and unsuccessful, taking hours or days, if producing a usable slurry at all. Owing to the many variables involved, a complex balance that must be achieved with a planetary ball mill to ensure mixing media do not become 'stuck' in ineffective patterns. Because it was known that difficulty in mixing was not a material compatibility issue, and could be overcome by the right mixing parameters, a DOE was planned.

Taguchi Planetary Ball Mill DOE

Optimization of the planetary ball milling process covered four variables, and was done using a Taguchi Design of Experiments (DOE) model. The Taguchi model gives an efficient method of testing many variables, and testing these on more than two levels. The capability of testing on more than two levels is a significant benefit over basic factorial models, as trends in main effects and features such as inflection points can be found. The four factors chosen for the DOE were mixing speed, ball to powder mass ratio, solids volume fraction, and fraction of water pre-mixed in the powder. Mixing speed was measured in rpm, and had a value of either 240, 360, or 540. Ball to powder mass ratio varied from 1:1 to 2:1 to 4:1, and solid volume fraction from 40% to 45% to 50%. In early testing, it was observed that some slurries, which seemed clumped, solid, and dry, would suddenly become a very low viscosity liquid with the addition of a very small amount of water. This prompted experimentation with the fourth variable, pre-mixed water fraction.

The desired fraction of water was added (either 80%, 90%, or 100%) and mixed on the ball mill for 5 minutes before the remainder of the water was added, if any. The response factors for the DOE were mixing time, printability, and sintered density. Mixing time was measured in minutes until a fully liquid slurry was achieved. Printability was measured by the ability of the slurry to be extruded consistently, without clogging, and maintain the intended geometry on the print bed. Sintered density was measured by percent theoretical density of bulk alumina.

For a 4 factor, 3 level design, the Taguchi method can generate a DOE consisting of as few as 9 samples (known as an L9). This was the method used in this research, and the main effects of each factor was plotted for each response. The samples were run in random order to further reduce the chance of self-selection or other systematic effects.

Taguchi Orthogonal Array Design
4 factor, 3 level, L9 = 9 runs

Table 1: Taguchi Slurry Mixing DOE

SAMPLE	MIXING SPEED (360, 240, 540)	BALL:POWDER (1:1, 2:1, 4:1)	VOL% (40, 45, 50)	% WATER (80, 90, 100)	MIX TIME (MINS)	SINTERED DENSITY	PRINTABILITY
1	1	1	1	1	100	63.75%	0
2	1	2	2	2	60	77.89%	1
3	1	3	3	3	60	83.82%	1
4	2	1	2	3	300	73.89%	0
5	2	2	3	1	1030	79.13%	0
6	2	3	1	2	60	64.50%	0
7	3	1	3	2	135	79.06%	0
8	3	2	1	3	30	84.31%	0
9	3	3	2	1	30	80.27%	1

Different printability and sintered density were observed due to coagulation rate, spreading, clogging, homogeneity, and aeration. In Figure 19, the main effects of each level for the four factors is shown for each response. The vertical axis of each plot represents the respective response variable, and data points represent the average relative effect across

all samples with that condition. For example, in the main effects plot for mixing time, data point #2 in the ball:powder factor corresponds to ~120 on the vertical axis. This shows that the effect of a 2:1 ball:powder mass ratio was to push mixing time far above that which was observed for 1:1 or 4:1. In this case, a lower value for mixing time was desired; for printability and sintered density, a higher value was always preferred. The optimum value for each factor is presented in Table 2.

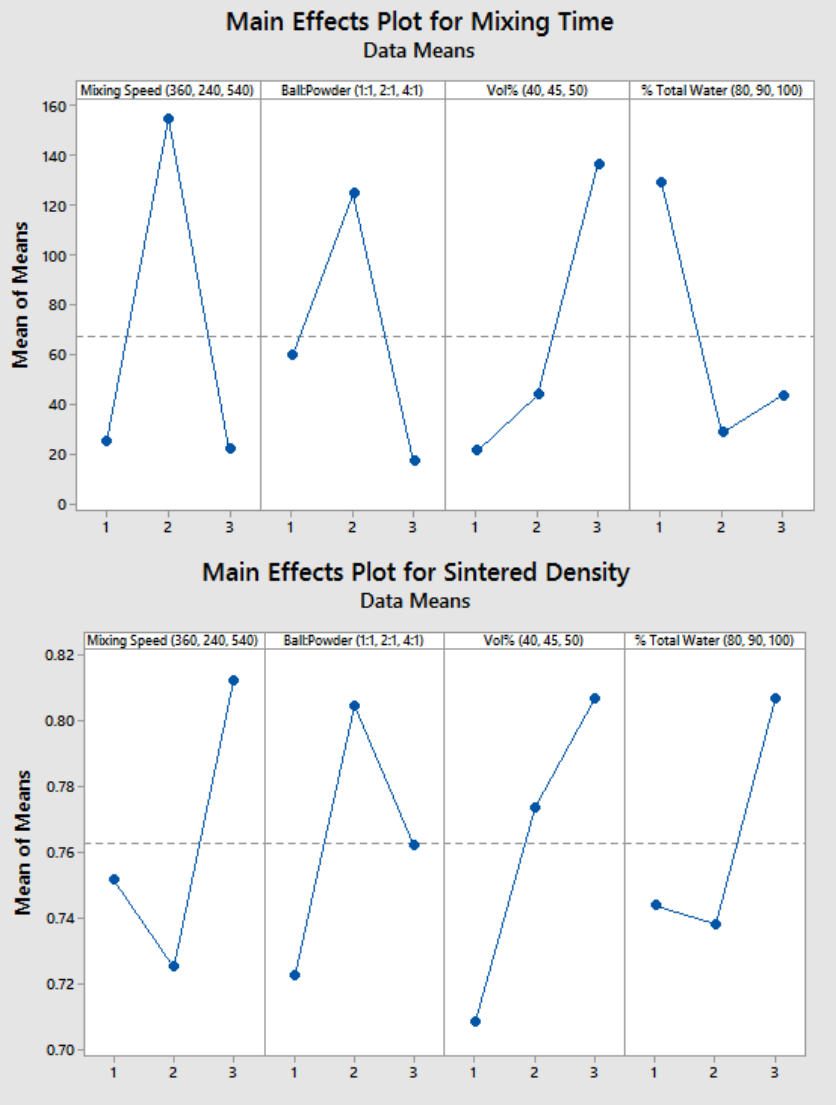

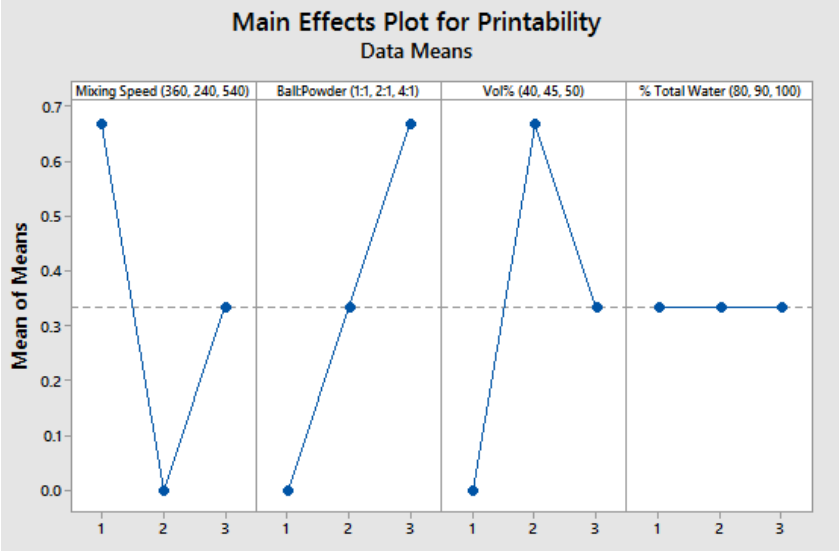

Figure 19: Mean Effects Plots for Mixing Time, Printability, and Sintered Density

Table 2: Taguchi DOE Optimum Values

Optimum values of each variable for the desired effect

Desired Effect	**Mixing Time**	**Printability**	**Density**
Mixing Speed	540	360	540
Ball:Powder	4:1	4:1	2:1
Vol%	40	45	50
% Water	100	-	100

With the end goal being a printable slurry that can achieve full density, a few compromises had to be made. In the end, the optimized standard mixing procedure used mixing parameters of 540 rpm, with 4:1 ball:powder mass ratio, 50 percent solids, and all of the water added. With these parameters, it was possible to mix slurries in 2 hours, with ideal printability, and sintering to above 99% relative density.

3.2 Investigation of Various Printing Methods

The decision to pursue direct coagulation printing (DCP) as the most promising new method of ceramic AM was made only after evaluation of multiple other candidate methods. Each of these methods was investigated with respect to maximum solids content,

printability, and sinterability. Only DCP showed promise in all three of these evaluations. For this reason, the highlights of the chitosan and PVA methods are discussed first, followed by a comprehensive discussion of the development of the DCP method.

3.2.1 Chitosan Gel Network

As the first method to be tested, the chitosan bio-polymer method provided exciting results, but was replaced relatively quickly by the more promising PVA and direct coagulation methods. The chitosan solution was found to carry up to 42 vol% Al_2O_3 when mixed by hand. This value was low enough to raise suspicion about the capability to be sintered to full density. In this state, prior to the addition of GDP, the slurry exhibited a viscosity of approximately 7000 cP, after which point it exceeded that maximum measurement capability of the instrumentation.

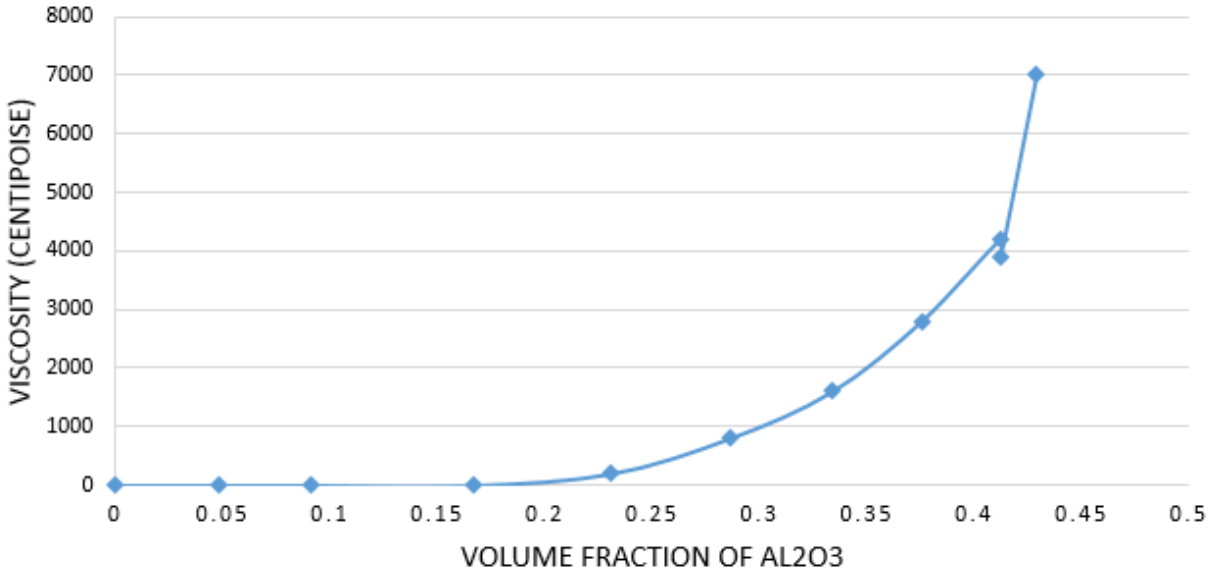

Figure 20: Viscosity vs. alumina solids content in chitosan/acetic acid solution. Points up until #5 were below the measurement threshold of the spindle being used. Reduction in viscosity at ~42.5 vol% is due to addition of 0.5 wt% ethanol as dispersant

The relatively low viscosity at this solids loading gave much confidence for printability. It was presumed that higher solids loading could be achieved with higher

energy mixing methods if sintering produced unacceptable densities. Once GDP was added, the gel network was formed in a matter of seconds, significantly raising the viscosity to that of a paste. In this state, the suspension was still extrudable, and was able to retain the desired geometry when printed, including overhangs and bridging small gaps (~6mm).

After printing however, the slurries required a very long time to dry, on the scale of hours to days, and could not be moved during this time. Slow drying, along with the large amount of impurities needing to be removed prior to sintering, and the cost of GDP discouraged further testing. Samples were never sintered. Instead, research turned to focus on the more promising methods of using a PVA binder and DCP, which were being developed simultaneously.

An image of the gel networks, or sponges, formed by GDP induced crosslinking of the chitosan without any alumina is shown in Figure 21.

Figure 21: Chitosan sponges without alumina

3.2.2 PVA Binder

The samples made with a PVA binder resulted in highly stabilized suspensions with good viscosity for extrusion and such high stiffness to be capable of extended bridging. This

material system exhibited a long handling life, but could be easily forced to harden and dry through exposure to elevated temperature. Drying times could be reduced from minutes at room temperature to seconds at 80°C. This was by far the easiest slurry for extrusion, as clogging in the nozzle was never an issue, and the slurry maintained the exact shape in which it was extruded, without noticeable spreading. Another incredible characteristic of the PVA binder system is that it could be extruded horizontally through space without any support structure underneath for at least twice the width of the extruded bead. As long as it was contacting another feature, even just on the side, the extruded bead showed very little deflection, and would harden fast enough with elevated temperature, that very complex features could be created. Because these extrusions were done by hand, geometric accuracy is poor, but Figure 23 shows multiple heat exchangers that were all printed in the orientation shown, with extremely long bridges between features and overhangs printed without support structure.

Figure 22: Structures printed in 1st iteration PVA binder testing

Solids loadings up to 50 vol% were achieved. Parts were sintered at 1550°C for 2.5 hours. Sintered relative density ranged from an average of 63% to 80%, depending on solids and PVA content. Initial PVA content was 19 vol% with respect to alumina and resulted in samples with an average relative density of 63%. This is in the range of green density for a part printed by direct coagulation. The high porosity indicated that there was likely too much PVA for good consolidation during drying, resulting in particle networks incapable of complete densification. Some parts printed by this method are shown in Figure 22, demonstrating excellent shape control, layer adhesion, and bridging capability.

The next iteration of testing used half the amount of PVA, bringing it down to 8 vol%. Part printability was essentially unaffected, and samples sintered at 1550°C exhibited an average relative density of 80%. The sinterability of these samples was obviously enhanced by a reduction in PVA. The density was still at least 10% below average for DCP samples. This showed that the required energy for densification was higher, however, there was no sign that this was the maximum achievable density. With an optimized sintering cycle, likely higher temperature and longer hold time, and potentially even less PVA, it is probable that full density could be achieved.

Figure 23: High temperature heat exchanger concepts with PVA binder

3.2.3 Direct Coagulation with TAC

The DCP method was identified as the most promising candidate to meet the specific aims of this research at an early stage. This led to a significant amount more optimization and therefore a much wider spread and more improvement upon results than with the chitosan or PVA methods. Most of the work can be divided into a few sections: reproduction of literature, TAC concentration experiments, and pH modification experiments. Each of these stages led to a realization of the fundamental principles affecting part printability and production.

Reproduction of literature taught about the ability of TAC to cause coagulation on its own. Attempts to recreate the results of direct coagulation casting experiments in literature [23] resulted in the discovery that, after initial mixing of the alumina, TAC, and DI water, the slurry was prone to rapid hardening when exposed to ambient atmosphere. It was not noted in the literature whether or not samples were exposed to atmosphere during processing, but because this effect was never mentioned, this characteristic is presumed to be undiscovered until now. Once this effect was realized, the subsequent processes in the reproduction of the literature were foregone, as the rapidly hardening slurry with TAC contained less contaminants and already behaved relatively ideally for printing. The slurry was studied extensively under these conditions. Experiments were run to optimize mixing time and quality, printability, and sintered density. The results of the very first printability and density experiment is shown in Table 3 below, where effects of print bed temperature and geometry are seen in the resulting coagulation time and sintered densities of parts.

Table 3: Early Printability and Sinterability Experiment

GEOMETRY	TEMPERATURE	COAGULATION TIME	SINTERED DENSITY
SINGLE DROP	**70°C**	**>30 seconds**	**64.76%**
MEDIUM DROP	**70°C**	**~30 seconds**	**96.51%**
~1 ML DROP	**70°C**	**~45 seconds**	**92.98%**
7 LAYERS	**70°C**	**30-40 seconds per layer***	**89.85%**
SINGLE DROP	**Room Temp (~21°C)**	**~4 minutes**	**32.09%**
MEDIUM DROP	**Room Temp (~21°C)**	**~5 minutes**	**91.21%**
3 LAYERS	**Room Temp (~21°C)**	**~4.5 minutes per layer***	**88.85%**

Figure 24: Parts from early printing experiments

This experimentation progressed and continued to show the promise of TAC as both a dispersant and a coagulation agent, which naturally became a cornerstone of the DCP method. The proposed mechanism for these phenomena is discussed in detail in Section 3.4 Investigation of Direct Coagulation Printing.

Shear Behavior

While no quantitative data was taken, observations were made on the effects of TAC concentration on the shear behavior of the material. When TAC was increased from 0.3 wt% to 0.5 wt% in a 50 vol% slurry, a substantial increase was observed in pressure required for extrusion. At 0.3 wt% TAC, the suspension seemed to behave as a Newtonian fluid, similar to water. When 0.5 wt% TAC was used, the suspension first appeared to have the same fluid properties (when under relatively low shear rates). However, upon extrusion or stirring, it was found that the suspension was extremely shear-thickening, or dilatant. This behavior is not conducive to extrusion in general, as the material must flow

under shear, instead of becoming more rigid. The suspensions with more TAC also exhibited a much slower rate of drying and hardening, which is also not desirable for AM.

Shear thickening behavior is commonly attributed to concentrated, non-aggregating suspensions. This is likely due to 'jamming' as the particles are forced from a relatively ordered structure to a random orientation under shear. The electrostatic forces between them strongly resist contact or shortening of the interparticle distance, increasing viscosity as shear rate increases [42], [43]. Under the assumption that these were the active mechanisms in the experimental suspensions, it can be postulated that the electric double layer (EDL) interaction energy was raised sufficiently to completely stabilize the suspension and cause significant resistance to shear through the addition of TAC. As the coagulation effect is desirable for DCP, and slurries should exhibit shear thinning behavior for extrusion, it was determined that 0.3 wt% TAC was preferable over 0.5 wt%.

Fractional Factorial DOE

A fractional factorial Design of Experiments and ANOVA were done to determine the main effects of many variables in the mixing and printing process, with a special interest in pH. In this study, print bed temperature, nozzle diameter, flow rate, and slurry pH, solids content, and TAC concentration were varied between a 'high' and a 'low' value. The DOE was a 1/8 fraction, single block, 6 factor design with Resolution III, and 8 total samples run. In this scenario, some of the main effects may be confounded with two-way interactions, but the efficiency of the testing is great enough to justify the time spent. Table 4 shows the DOE with the corresponding 'low' and 'high' values for each factor. Flow rate was measured in percent of the arbitrary value used for ABS extrusion in the Cura slicer engine. The DOE was prepared in Minitab 17.

Table 4: DCP 6 Factor Design of Experiments

RUN ORDER	TEMP	PH	VOL%	WT%	FLOW RATE	NOZZLE DIA.
1	-1	-1	1	1	-1	-1
2	1	-1	-1	-1	-1	1
3	1	1	1	1	1	1
4	1	-1	1	-1	1	-1
5	-1	1	1	-1	-1	1
6	-1	-1	-1	1	1	1
7	1	1	-1	1	-1	-1
8	-1	1	-1	-1	1	-1
LOW	**Room Temp**	**pH 3**	**35 vol%**	**0.3 wt%**	**30%**	**0.6 mm**
HIGH	**65°C**	**pH 8.7-9**	**50 vol%**	**0.5 wt%**	**50%**	**1.2 mm**

Samples were scored during printing and after sintering according to observed spreading after extrusion, coagulation time, green strength, sintered density, and shrinkage. Scores for printing parameters were qualitative, while measured values for sintered density and shrinkage were used. These scores were given weights with respect to importance in optimizing the printing process, as shown in Table 5. Scores for samples in all categories were summed to give an overall score which could be analyzed using ANOVA techniques in Minitab. The main effects of each factor are presented in Figure 25.

Table 5: DCP 6 Factor DOE Score Weights

SCORING METRIC	SPREADING	COAGULATION RATE	GREEN STRENGTH	SHRINKAGE	SINTERED DENSITY
RELATIVE WEIGHT	0.5	4	1	3	0.5

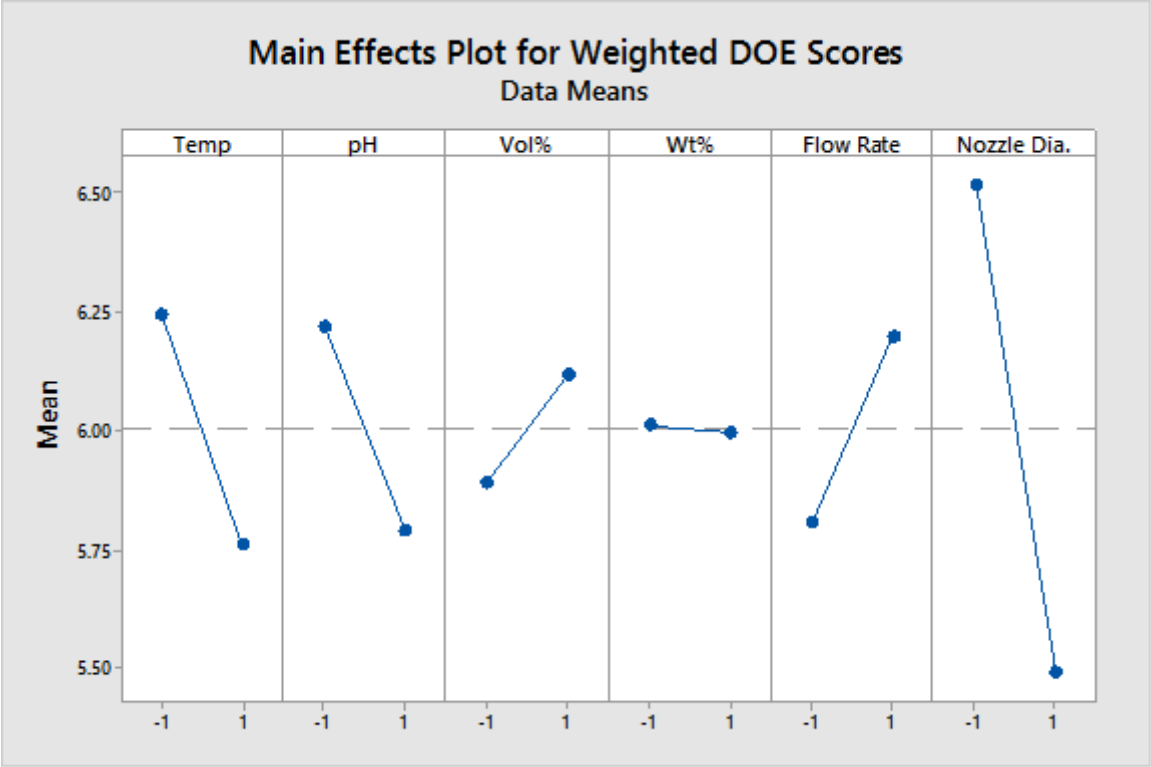

Figure 25: Main Effects Plot for Weighted DCP DOE Scores

From Figure 25, it is clear which value produced the best results for each factor; according to this, the optimized slurry for DCP would be made with 50 vol% alumina, 0.3 wt% TAC, be adjusted to pH 3, and be printed at room temperature through a 0.6 mm nozzle, at a relatively high flow rate. Further adjustments to this were made to accommodate other responses such as required extrusion pressure and over-extrusion by adjusting pH to 4-4.3 to lower viscosity and bringing flow rate down slightly.

3.3 Investigation of Sintering Parameters

When first making parts, a baseline sintering schedule is established around the melting temperature of the material and past experience, which is then modified with respect to results. As sintering is generally governed by diffusion, it follows the Arrhenius relationship, increasing logarithmically with temperature and linearly with time. Because

it may not always be practical to increase sintering temperature, the time may be the only tunable factor. Improvements in the sintering schedule were made until a maximum part density was achieved.

Initially, all experiments were done using Taimei TM-DAR 100nm powders. Parts made with TM-DAR were initially sintered according to an arbitrarily selected schedule having a maximum temperature of 1500°C and a hold time of 1 hour at that temperature. From this point, attempts to optimize the sintering schedule were made, with the goal of achieving full density.

During the process of tuning the mixing and printing of DCP slurries, powder suppliers were switched due to cost and availability. It should be apparent from information in Section 1.2 DLVO Theory Overview, that sintering behavior is strongly affected by powder size and morphology. The transition from Taimei 100 nm powder to SkySpring 150 nm powder resulted in a significant change in the sintering parameters after optimization with the former. Using SkySpring powders, research started with the sintering schedule that had been developed for Taimei powders as a baseline to compare the sinterability of the two systems. During experimentation with the SkySpring powders, pH modification was introduced, introducing the likelihood that the structure and attractive forces in particle networks in green parts may also have been modified. This introduces a variable that was not tested on Taimei powders, however the general difference in sinterability can still be elucidated from the results in Table 6.

Table 6: Results of Sintering Study

SINTERING SCHEDULE	AVERAGE RELATIVE DENSITY
1500, 1 HR, TM-DAR	79.47%
1550, 2 HRS, TM-DAR	87.88%
1550, 2.5 HRS, SS150	66.94%
1750, 4 HRS, SS150	96.64%
1600, 16 HRS, SS150	95.19%

The initial sintering schedule used with TM-DAR powders produced relatively low density parts (~80%); however, any concerns about sinterability of the material system were quickly allayed with the second schedule. Increasing maximum temperature by 50°C and doubling the hold time, an increase in density of almost 10% was observed. These sintering temperatures are well within the bounds of normal processing for alumina parts [23], [44]–[47], so confidence in the ability to reach full density with slightly higher temperature and longer hold time was high.

Upon switching to SkySpring powders, it was predicted that the required energy would be higher due to the larger particle size. The sintering schedule was adjusted to have a 25% longer hold time. This resulted in parts with the lowest observed densities of the entire study (~65%). In an attempt to ensure that the SkySpring powders would be sinterable to full density, the schedule was adjusted to significantly increase the energy input. After increasing temperature by 200°C and hold time by 1.5 hours, parts were produced with an average of about 96% relative density; high enough to ensure full density was achievable with these powders. After this, an attempt was made to develop a lower temperature sintering schedule to accommodate a wider variety of furnaces. Reducing temperature to 1600°C and increasing hold time to 16 hours, parts with practically equivalent densities were manufactured.

All density measurements for these results were done by Archimedes method. This method has inherent inaccuracies due to the method of sealing parts against water uptake, and can result in calculation of lower-than-actual density. Areal density measurements were made on select parts made with SkySpring powders and sintered at 1750°C and 1600°C, with results showing densities from 97-100%. This confirmed that these sintering schedules did indeed produce fully dense parts.

3.4 Investigation of Direct Coagulation Printing

The work presented in this section was submitted for publication in the peer-reviewed journal Additive Manufacturing, and was left as submitted, to retain the intended flow of thoughts and information[1]. For this reason, some explanations and processes may have already been mentioned, however, it is also hoped that this can reinforce the understanding of the work presented through differences in wording and train of thought.

3.4.1 Journal Submission Summary

This work investigates the feasibility of a binderless, extrusion-based additive manufacturing approach to fabricate alumina (Al_2O_3) parts from nanopowder. Traditional manufacture of ceramics with subtractive methods is limited due to their inherent hardness and brittleness, inevitably leading to ceramic parts with less-than-optimal geometries for the specific application. With an additive manufacturing approach, ceramic parts with complex 3D geometries, including overhangs or hollow enclosures, become

[1] Additive Manufacturing of Ceramic Nanopowder by Direct Coagulation Printing
Tucker J. Hensen, Trevor G. Aguirre, Corson L. Cramer, Austin S. Wand, Kaka Ma, David A. Prawel, John D. Williams, Troy B. Holland
Colorado State University, 80523 Fort Collins, CO, USA

possible. These complex ceramic parts are highly valuable in heat exchanger, condenser, biomedical implant, chemical reactant vessel, and electrical isolation applications. This research employed direct coagulation of alumina nanopowder slurries with the polyvalent salt tri-ammonium citrate providing the solidification mechanism in an extrusion-based printing process. The viscosity of the slurries was modified by adjusting pH, resulting in a paste that is suitable for extrusion, which retains near-net geometry. It was shown that the direct coagulation approach can be used to create a suspension with tuneable flow characteristics and coagulation rate, and a mechanism describing the process was proposed. The direct coagulation printing (DCP) method is described in detail, including how slurry is extruded, solidified, and printed in complex geometries, and sintered to full density. Microstructure and mechanical properties were characterized with a comparison to different materials and methods from literature.

Keywords: Additive Manufacturing (AM), Binderless, Direct Coagulation, Extrusion, Nano

3.4.2 Introduction

Additive Manufacturing (AM) has spurred a wave of new capability in the world of design allowing for novel and optimized designs that were not previously attainable [3], [4], [7]. Specifically, extrusion-based 3D printing is one of the most cost effective methods of additive manufacturing and is capable of producing functional parts with polymers, metals, ceramics, and composites [9], [28], [29], [48]–[54]. 3D printing of ceramics allows for engineering of complex with optimized geometry, as well as thermal, electric, and mechanical properties. This capability leads to increased performance of lightweight structural components, operation of thermal energy generation systems, sensors, biomedical devices, and so forth [4], [11], [30], [31], [55]–[57]. With its many advantages,

development of ceramic AM technology has been pursued essentially since the age of ceramic pottery. Robotic controls were first used to deposit ceramics in the 1990s [3], [56]. Common methods of AM with engineering ceramics include binder jetting, stereolithography (SLA™), direct ink writing (DIW), selective laser sintering/melting (SLS/SLM™) and laser chemical vapor deposition (LCVD) [4], [49], [54]. The scope of the current work focused on an extrusion-based system.

The use of nanometric precursor powders for AM has been found to drastically improve sinterability due to enhanced thermodynamic driving forces for diffusion arising from small radii of curvature at surface interfaces and increased surface area. Mechanical properties such as flexural strength can be considerably improved when sintering is tuned to keep final grain sizes in the nano-scale as well [1], [5]. This has been demonstrated in previous work, resulting in high density alumina parts with good mechanical and electrical properties relative to traditionally manufactured alumina [44], [58]. Nano alumina is also small enough to be capable of colloidal dispersion, and is widely used in this way for slip and tape casting as well as abrasive polishing [5], [59]–[61]. These colloidal suspensions have also been used in extrusion based AM by a few groups [2], [12], [26], [27], [62], [63] with promising results, however, none have employed a binderless system such as the direct coagulation method described in the current study.

Previous studies have shown that fully dense parts with complex geometries produced by the direct coagulation approach exhibit mechanical properties comparable to parts made by conventional methods [45], [64]–[68]. Some groups have used tri-ammonium citrate (TAC) as a dispersant for gel-casting and laser sintering [22], [46], [57], [69], [70]. It is known that slurries of alumina and other ceramic material can be directly

coagulated by adjusting the pH [24], [71]. An opportunity to print virtually any ceramic or metal in nanopowder form without binders is presented by using TAC as a dispersant, using the direct coagulation method for additive manufacturing, and subsequent sintering. This makes the process more time and energy efficient because there is no burnout step. Direct coagulation printing (DCP) is also less prone to impurities than methods requiring a binder [3], [4], [9].

DCP falls under the category of extrusion freeforming (EFF) techniques, which encompass such other technologies as fused deposition modeling (FDM) and robocasting (RC). An early paper done by Cesarano et al. [26] defined the term robocasting, which is most closely comparable to DCP. The novel differences are that DCP does not use binders, and is focused on the coagulation effect, rather than drying. This study investigates the feasibility of DCP as a method of ceramic additive manufacturing, including making the printing material, establishing printing parameters, characterizing media flow and coagulation behavior, establishing sintering schedules, analyzing microstructure, and testing mechanical properties. Free sintering of nano-sized alpha-alumina from powder compacts used in [44] helped to establish sintering parameters in this research. We believe this is the first reporting of 3D printing of ceramics without a binder, starting from nanopowder, and using the direct coagulation printing method with an extrusion delivery system.

The fluid-to-solid transition of DCP is controlled by pH shift in an aqueous ceramic slurry with the polyelectrolyte dispersant/coagulant TAC resulting in coagulation of particles out of colloidal suspension, similar to the high valence counter-ion direct coagulation casting method and others [16], [23], [24], [46], [72], [73]. DCP involves an

aggregation process as the ceramic particles in suspension become unstable due to reduction of zeta potential and changing ion concentration in an *in situ* chemical reaction. DLVO theory of colloid stability can be used to analyze this as a symmetric system with homoaggregation [36], [74]–[76]. The citrate ion in TAC is a multivalent ion, with charges ranging from -1 to -3 eV, as ammonium ions dissociate with increasing pH [24]. The three pK_a values of TAC are at pH 3.1, 4.8, and 6.4; therefore, at the slurry's natural pH of 8-9, about 5-6 orders of magnitude more positive ions are present at the natural pH than at pH 3. At the natural pH of 8-9, citrate ions have a valence of 3, and Debye length is at its shortest. Coagulation is very rapid, occurring in seconds at this pH. This follows the Schulz-Hardy rule, which states that salts are most effective at destabilization of colloids when valence is high [36]. When pH is shifted to the acidic range, ammonia evaporation is reduced as a result of reduced ammonium ion dissociation, slowing the evaporation of water and allowing for longer coagulation time. The increase in viscosity decreases diffusion throughout the slurry, further increasing coagulation time and working life.

Interparticle relationships and ammonia evaporation rate based on DLVO theory were calculated using Equation 8, where φ is the double layer force, z is the valence of the respective ions, e is the electron charge, ε is the dielectric constant of the medium, ε_0 is the permittivity of free space, and δ is the interparticle spacing. Equation 9 is the Van der Waals force (ϕ), where A_H is the Hamaker constant and R_s is the particle radius. Equation 10 is the Debye length (κ^{-1}), z_i is the counterion valence, and c_i^{∞} is the counterion concentration [77].

$$\varphi = \frac{z_1 z_2 e^2}{4\pi\varepsilon\varepsilon_0\delta}$$

Equation 8: Repulsive Double Layer Force

$$\phi = -\frac{A_H R_s}{12\delta}$$

Equation 9: Attractive Van der Waals Force

$$\kappa^{-1} = \{5.404x10\text{^}15 \sum_i z_i^2 c_i^{\infty}\}^{-1/2}$$

Equation 10: Debye Length

The unique effects of pH modification on colloidal slurries allow precise tuning of the viscosity and coagulation rate. This makes the DCP method very adaptable to a variety of printing conditions and printer styles.

3.4.3 Materials and Methods

Producing a fully dense, 3D printed part involves three main steps. First, a slurry is prepared with a sufficiently high solids content in order to avoid catastrophic shrinkage and be easily sintered to >97% theoretical density. Second, the slurry is printed to near-net shape. This step dictates that the material must have a sufficiently low viscosity for extrusion and must quickly become sufficiently stiff to retain the intended shape under its own weight. This, while also coagulating to form green parts that are strong enough to be handled for sintering. Third, the part is sintered according to an appropriate schedule to create the desired microstructure.

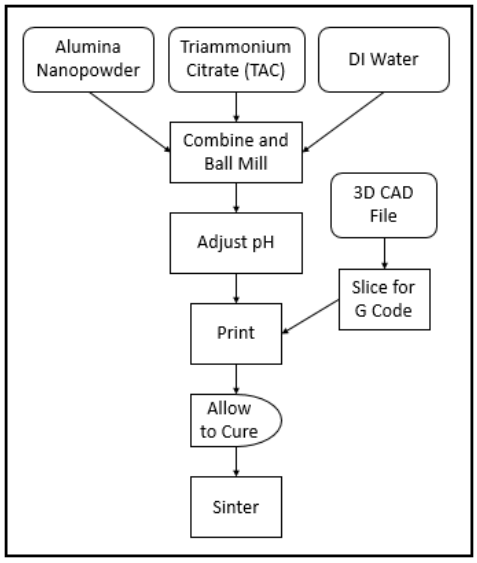

Figure 26: DCP Process Flow

Alumina slurries were prepared with 99.0% pure α-phase Al_2O_3 powders with an average particle diameter of 150 nm (Skyspring Nanomaterials, USA). Tri-ammonium citrate, 97% (titration), and molecular weight 243.22 g/mol (Sigma Aldrich, USA), was used to generate the direct coagulation. TAC is dissolved in de-ionized water at 0.3 wt% with respect to the alumina powder being used, before being added to the powders at the desired volume fraction (vol%). A high energy ball mill (HEBM) (PQN04, Across International, USA) was used with alumina ball milling jars with 10mm diameter alumina media at a mass ratio of 4:1 to powder mass. The jars had Viton gaskets, and were further sealed with parafilm and rubber tape to prevent the escape of any vapors arising during mixing. It was critical to the mixing process to ensure that the jars were well sealed. All processes after this point gave special consideration to minimizing the exposure of the slurry to unsealed, ambient atmospheric conditions, as this would induce premature coagulation due to ammonia or water evaporation. The sealed jars were then loaded, into the HEBM and milled for one hour of “on” time, with a repeating cycle of 5:5 minutes “on” :

"off", at 580 rpm. Slurries with low viscosity and a pH around ~9.10 were produced. The pH was adjusted to approximately 4.50 with 2M nitric acid (HNO_3). During pH adjustment the slurry thickened to a paste which did not deform under its own weight and required minutes to coagulate, as opposed to seconds.

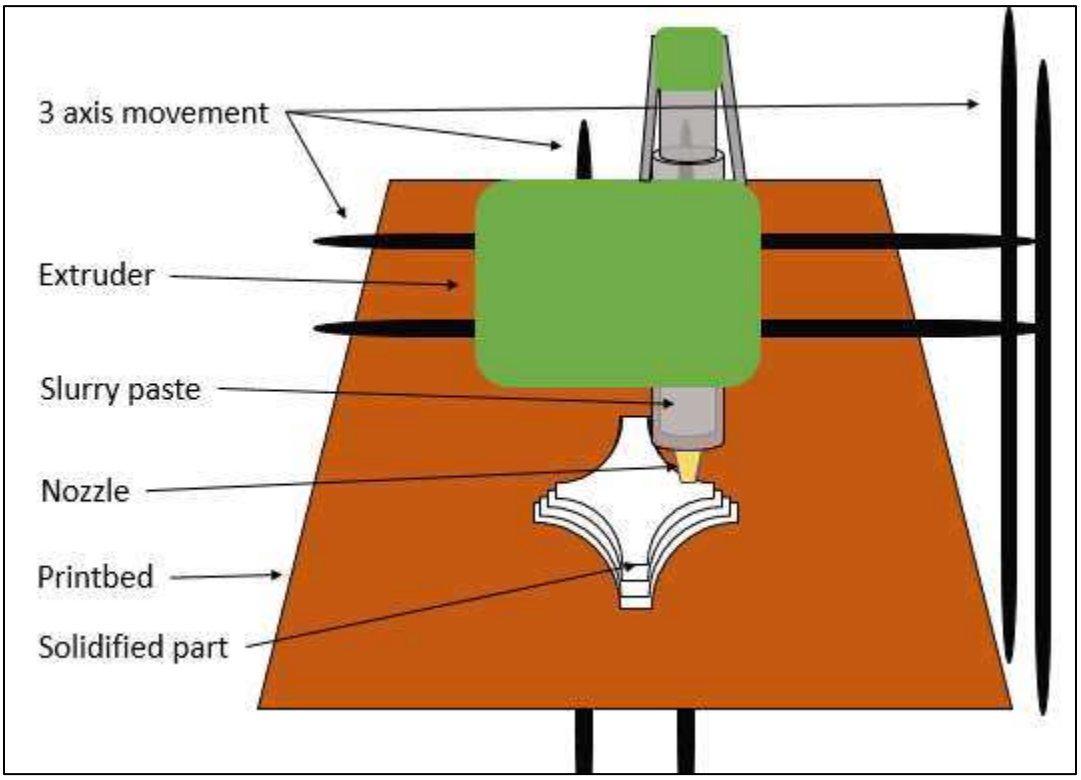

Figure 27: Diagram of DCP printer

After pH adjustment, the slurry was loaded into syringes in a custom extruder based on the open source model "Universal Paste Extruder", (RichRap, Thingiverse.com). The extruder was modified with a metal transmission to allow higher extrusion pressure for high viscosity slurry and smaller extrusion nozzles. The extruder was mounted on the gantry of a Lulzbot Mini 3D Printer (Aleph Objects, USA) with a glass print-bed. Machine control G-code for the printed parts was based on stereolithography files processed using the Cura slicer engine (Ultimaker, USA). The printer was placed in an enclosure to limit

temperature gradients and air flow that may disturb the printing process. Nozzles with an inner diameter of 0.6 mm were used. The parts were printed through a room temperature nozzle onto an unheated bed and allowed to cure before sintering.

Viscosity measurements were performed with a Viscolead Pro viscometer (Fungilab, Spain) with an L4 spindle and a shear rate of 132 s^{-1}. After curing, sintering of parts was performed in atmosphere in a high-temperature furnace (Thermolyne 4610, USA). The sintering schedule consisted of a fast (100°C /minute) heating rate to above 1200°C, followed by a slower ramp (25°C /minute) to a hold temperature of either 1500, 1550, 1600, 1650, or 1750°C, and held for between 1 to 16 hours according to maximum temperature. Samples were allowed to cool naturally in the furnace. No intermediate binder removal step was necessary between green and sintered states. Density of parts was found by both Archimedes and areal density methods [78]. Grain size was determined by digital image analysis of SEM micrographs of polished surfaces using ImageJ (Broken Symmetry Software). Specifically, the three-circle method was used according to ASTM E112. The average Vickers hardness was found by Vickers indent according to ASTM E384-16 using an HV1000Z Microhardness Tester (Pace Technologies, USA) with an applied load of 9.8 kgf and 15 seconds hold time. Flexural modulus and flexural strength were measured using four point bending according to ASTM C1161 on an Instron testing machine (Model 8501, Instron, USA) with a crosshead speed of 0.127 mm/min.

Zeta potential measurements were taken using a dynamic light scattering (DLS) instrument (Zetasizer Nano ZS, Malvern Instruments, United Kingdom). For these, alumina powder was mixed at 0.5 vol% in DI water, with various concentrations of TAC, and loaded into transparent cuvettes.

3.4.4 Results

Powder and Slurry characterization

Figure 28 is an SEM image of as-received powder showing uniform particle diameter of approximately 150 nm and roughly spherical shape, consistent with the manufacturer's specifications. Characterization of the coagulation and fluid properties of the slurry is critical to both quality and reproducibility in printing, so it is important for predictive ability to document the powder quality, size, and size distribution.

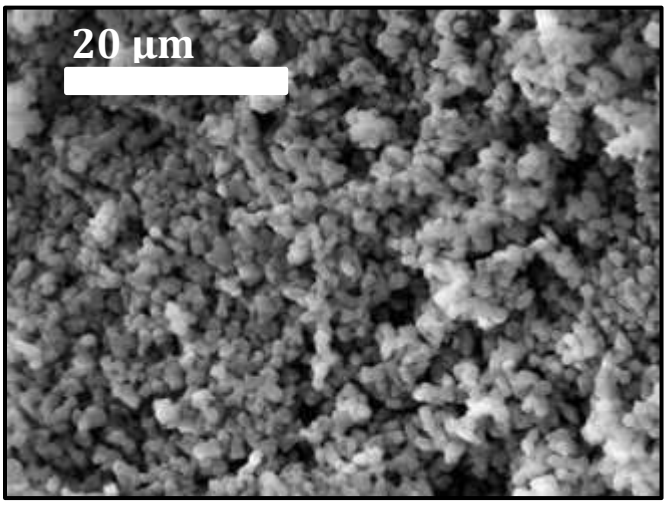

Figure 28: As-received alumina powder

TAC acts as a weak acid in aqueous solution and changes the electrical interactions between particles through modification of the electrical double layer force and Debye length; the effects of which are shown as derived from Equations 1-3 in Figure 29.

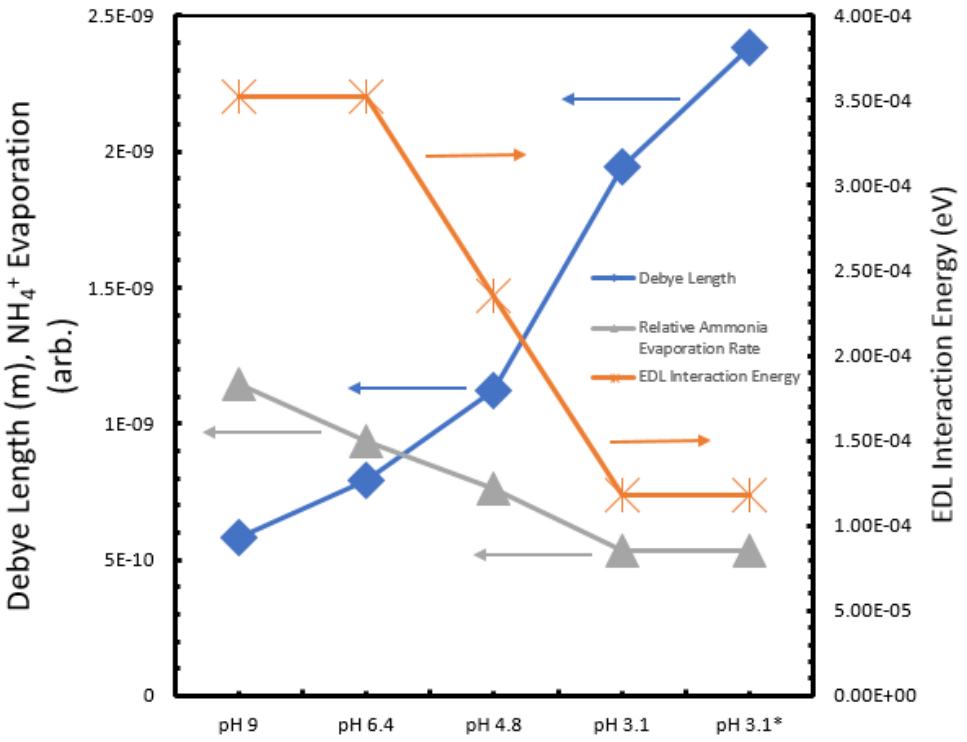

Figure 29: Analytical model of Debye Length, EDL Interaction Energy, and Ammonia Evaporation Rate vs. pH. * represents pH 3.1 after significant ammonia evaporation

The zeta potential of the alumina was measured with respect to TAC concentration and pH. It is shown in Figure 30 that the zeta potential magnitude increases steadily with increased TAC concentration, reaching a saturation value of -55 mV at concentrations above 0.8 wt%. Figure 31 shows that the zeta potential is positive around pH=2, decreases to zero, or the IEP, at around pH=4-4.5, and then becomes relatively large and negative as the slurry is adjusted into the basic region of pH. This is consistent with published results [24].

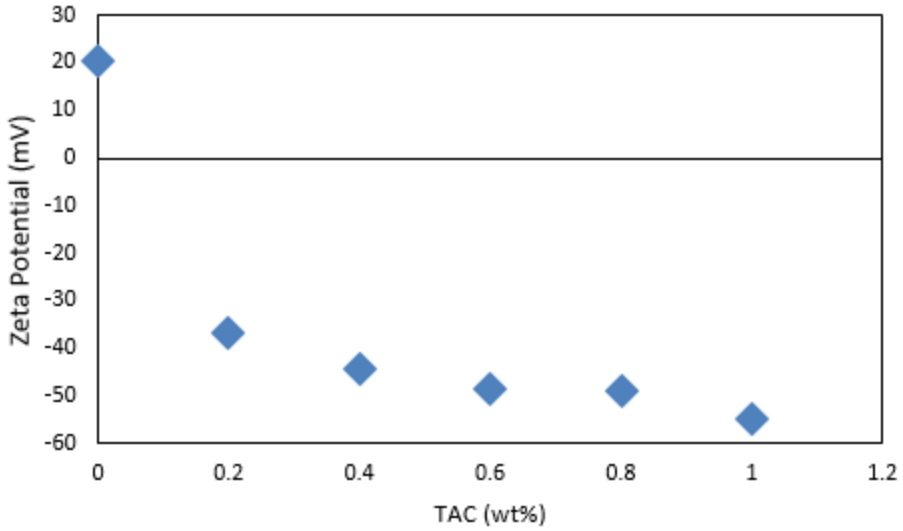

Figure 30: Zeta potential with respect to TAC concentration

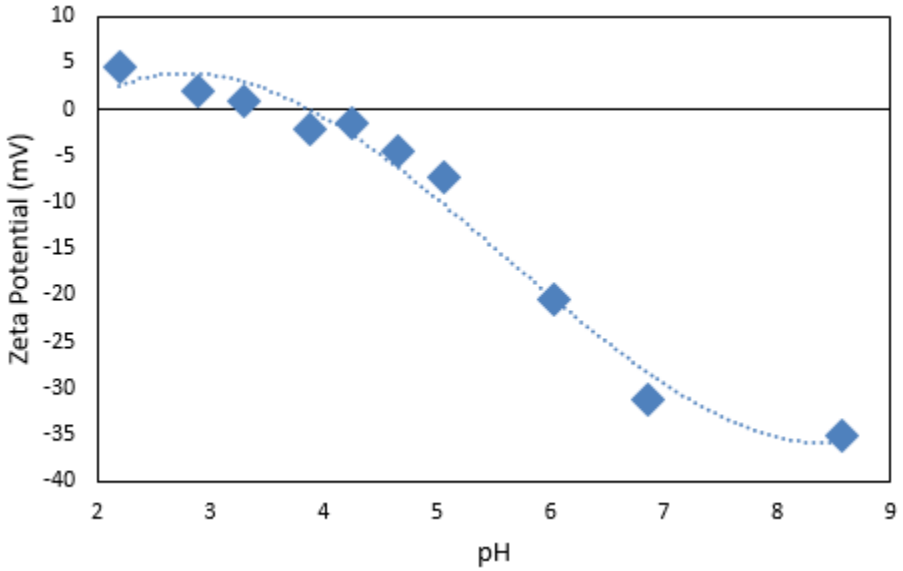

Figure 31: Zeta Potential with respect to pH

Figure 32 presents slurry viscosity plotted against slurry pH. As mentioned previously, pH was modified using 2M HNO_3. For the slurry prepared at 50 vol% alumina with 0.3 wt% TAC, the pH is initially near the IEP of alumina (pH 8-9) [24] and at its lowest viscosity, allowing the assumption that the mixture is at its most homogenous and well dispersed state. After the dissociated ammonium molecules from TAC are deprotonated to

form ammonia, the ammonia evaporates out of solution, as shown in Equation 11 causing a pH shift and change in electrical interaction forces between particles [23]. This effect leads to coagulation of the particles as the suspension moves into the unstable region.

$$NH_4^+ + OH^- \rightleftharpoons NH_3 \cdot H_2O \uparrow$$

Equation 11: Ammonia Evaporation Reaction

Using this principle, slurry extrudability and solidification behavior may be modified through pH adjustment. Viscosity changes little until pH is below 6.4, then increases nearly linearly until pH 3.1. For a nozzle diameter of 600 μm, optimal viscosity for extrusion was found to be between 750 and 1000 Pa·s, correlating to a pH between 4.00 and 4.30. This pH range also corresponds coincidentally to the IEP of the system, supporting the assumption that it is in this range that the strongest particle networks are formed due to lack of repulsive forces. In which case, it is possible that the resulting green parts would be of maximum strength and density for the system.

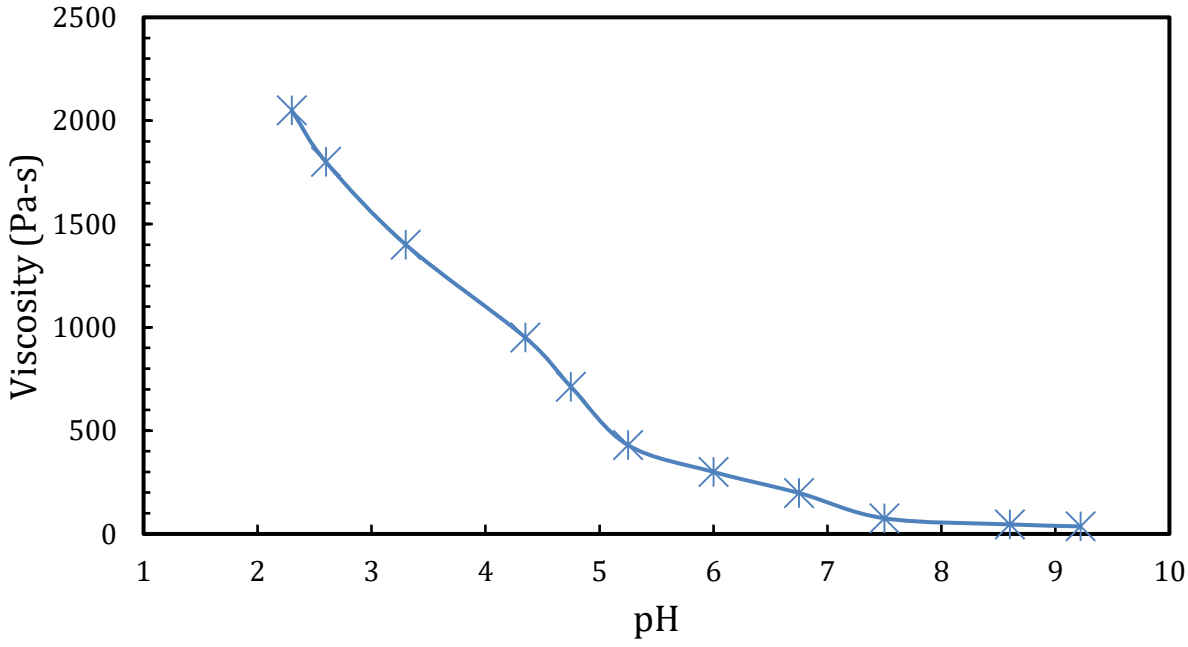

Figure 32: Slurry viscosity vs pH

Printing

Before parts were produced, printing parameters were established for the slurry. Volumetric flow rate, movement speed of the printhead, and print-bed temperature all influence the quality of parts being printed. Inadequate flow rate leaves incomplete and broken segments of material or causes the slurry to spread poorly. Inadequate movement speed causes slurries to coagulate and clog in the nozzle or coagulate too fast on the print-bed resulting in poor layer adhesion. It was found that a flow rate of 0.0028 cm^3/s paired with a movement speed of 10 mm/s with the print-bed at ambient temperature yielded the best layer adhesion, with the least spreading, and reducing cracking of parts, resulting in the best printing results.

Printed parts were evaluated by minimum feature size as well as green density, strength, cure time, and layer adhesion. Minimum feature size was found to be 620 μm, 20 μm of which was due to spreading after leaving the nozzle. Parts did not deform under their own weight implying that coagulation occurs. Green parts were, on average, 53% theoretical density with some samples as high as 65%. Green strength of parts was too low to be measured by the available load cell; however, green strength was sufficient for part removal from the build plate and handling without failure before sintering. As complete coagulation generally required longer than the time to print, it was prudent to allow time after printing to ensure sufficient green strength for removal and handling. This cure time was typically between 30 and 60 minutes for material extruded at pH ≈4.5. While individual layers may have acceptable microstructure and properties, if adhesion between layers is not complete, green strength, sintered density, and sintered strength are severely affected [28], [50]. Due to the nature of the coagulation process, particles in successive

layers likely form attractive networks with each other, resulting in excellent layer adhesion. As shown in Figure 33, a thin-walled part section shows homogenous bulk material with no observable separation between layers.

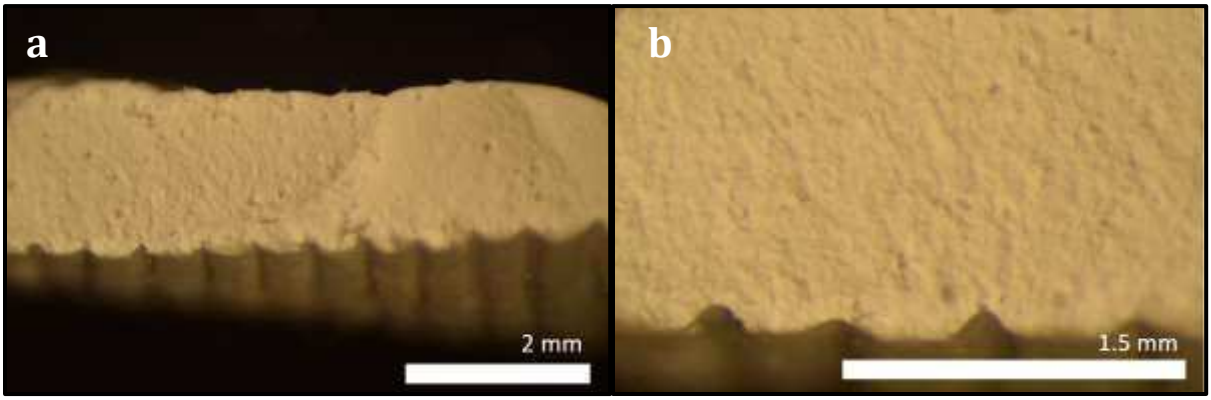

Figure 33: Fracture surface of a green part where a) is at 200x and b) is at 300x

Figure 34 contains photographs of several complex geometries that were printed. The DCP method of coagulation and extrusion demonstrates how overhangs can be printed with a hollow model rocket design. A closed-cell hollow part and fully dense turbine propeller prototype were also attained with this method. All of these parts were printed without the use of support material.

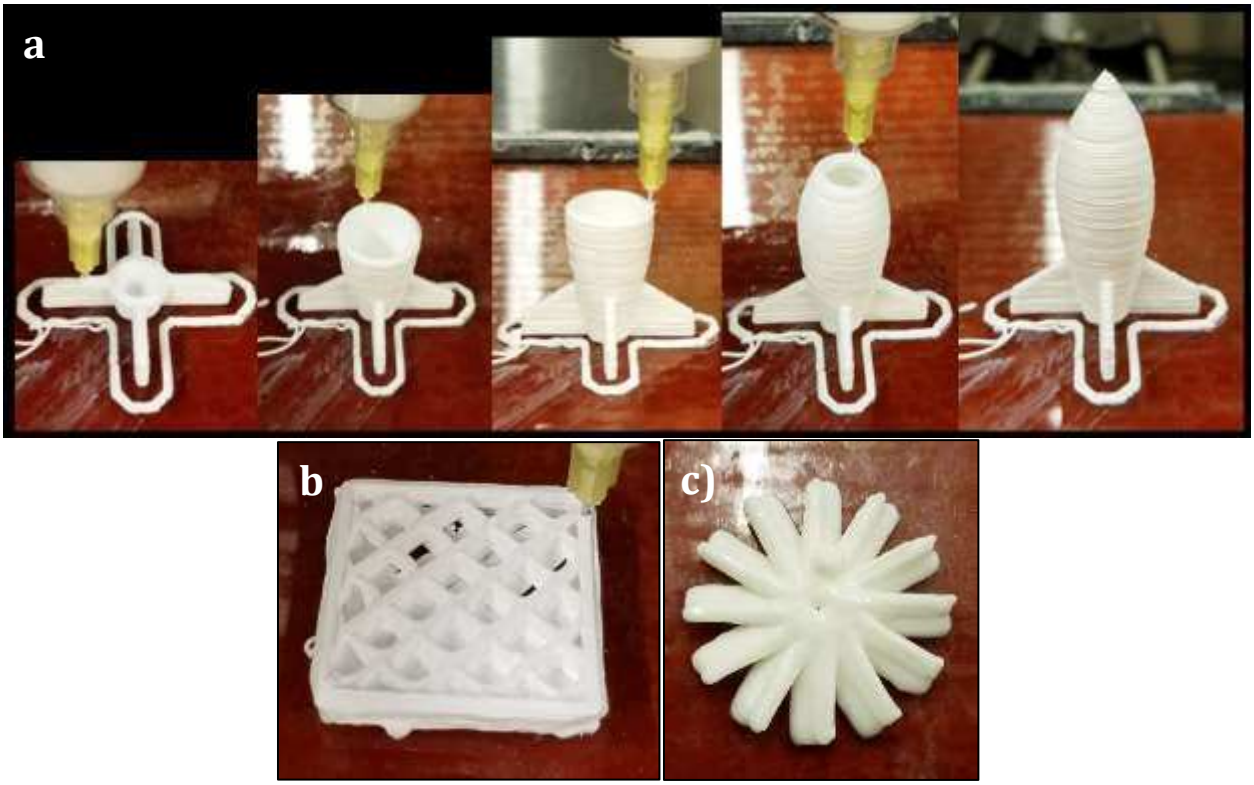

Figure 34: a) Printed rocket prototype demonstrating overhangs and enclosed volumes, b) part printed with closed-cell hollow infill, c) printed turbine propeller

Sintering

After free sintering in air according to previously mentioned heating schedules, densities of parts above 97% theoretical density were measured by both the Archimedes principle and areal methods. Areal density measurements were as high as 99.99% relative density. In addition to density, the microstructure of sintered parts was characterized in SEM, as shown in Figure 35. Grain growth was roughly isotropic, resulting in roughly spherical grains and limited porosity. Average grain size was 2.2 μm ± 1 μm across a range of samples sintered from 1500 – 1750°C for 1 – 16 hours.

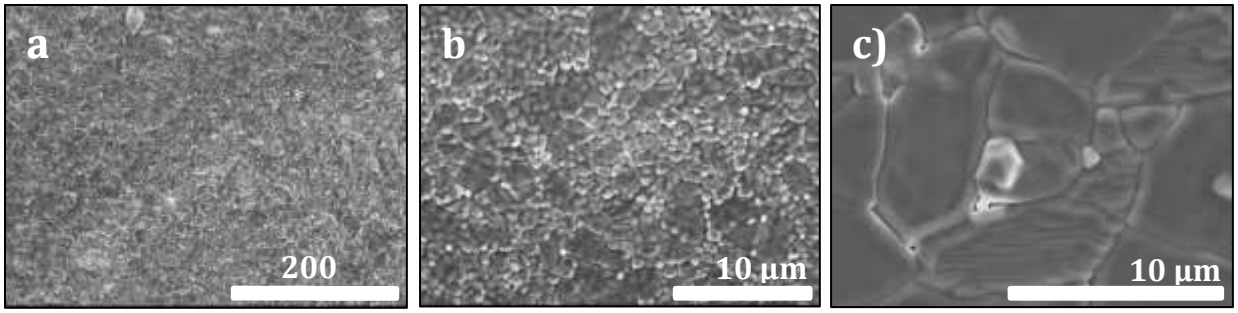

Figure 35: SEM images of sintered, 3D printed alumina showing magnifications of a) 250 x, b) 4,000 x, and c) 7,000 x

Sintered parts were translucent white, transmitting light through walls as thick as 2 mm, as demonstrated in Figure 36. This is further evidence of the high relative density and purity of the sample because of the sensitivity of optical properties of alumina to defects such as pores and impurities [47]. Part shrinkage due to densification was found by measuring at least four features on select parts before and after sintering. It was found that, among 15 samples, there was an average isotropic shrinkage of 19% with a standard deviation of 3%. Figure 36 shows a green part next to another that was printed identically and then sintered to full density. It is important to note that warpage, failure through cracking or rupture is possible if parts did not cure sufficiently.

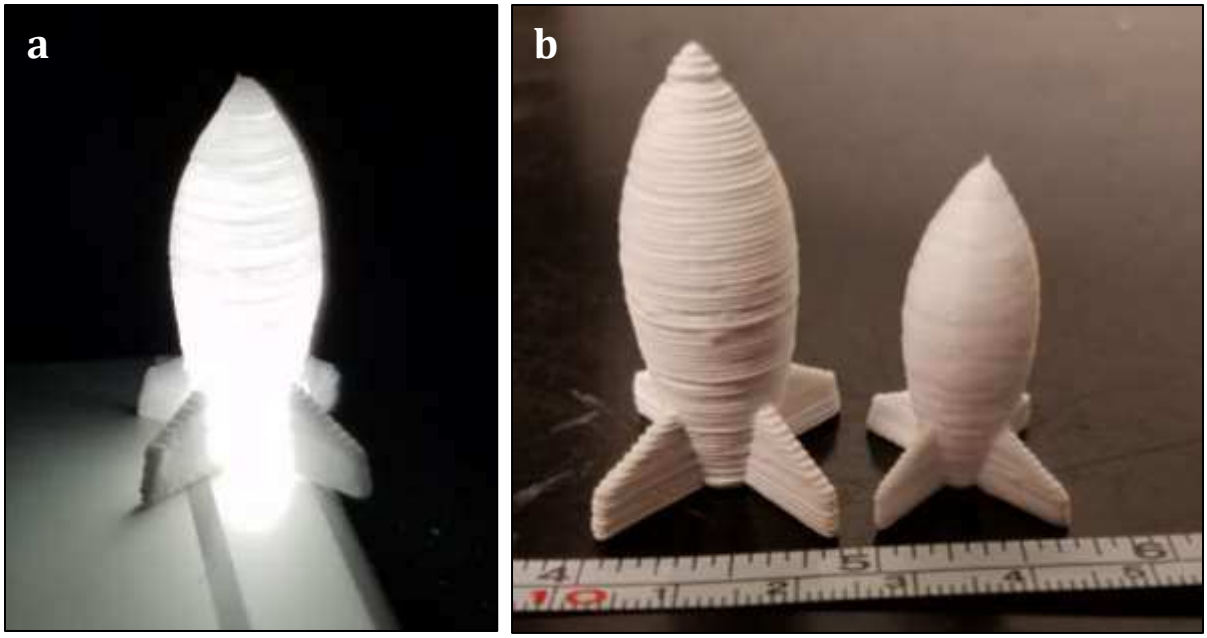

Figure 36: a) Sintered rocket translucent to white light, b) Identically printed green and sintered rockets demonstrating shrinkage due to sintering

Mechanical Testing

To assure comparability with bulk alumina, the mechanical properties of printed parts were measured. Samples displayed an average hardness of 1788 HV. Flexural modulus and flexural strength averaged 10.8 MPa and 173 GPa, respectively. Results found in this study were compared to published values from a wide range of industrial applications and minimum requirements [64], [65]. Specifically, nine commercial grades of alumina and two fine grained (1-2μm and 10-15μm) samples, produced by conventional sintering methods, are compared to direct coagulation samples. The nine grades are split into two main groups, the first being A1-A5, having relative densities of at least 99%; and the second group being A6-A9, with relative densities between 80% and 99%. These main groups can be divided into sub-classes according to type, purity, and intended service [66]. This study is comparing properties of conventionally fabricated parts to those made layer-by-layer. Layer-by-layer forming processes can result in macro-scale structural defects that

can affect the observed properties, regardless of the microstructure. Flexural strengths of parts produced by DCP were notably less than reported values for commercial alumina by a factor of ~20, as evidenced in Figure 37. The flexural modulus of printed parts, however, was very comparable to high-grade commercial alumina, with values as high as 400 GPa as shown in Figure 38. It can be seen from Figure 39 that hardness of printed samples was in the same range as the hardest commercial grades. Therefore, the printed parts have potential application in products requiring wear resistance, along with any applications for which mechanical strength is not of special importance, such as electrical insulation and refractory applications. Although low strength was measured, we note that very little tuning of the toolpaths or other printing parameters to improve mechanical properties was performed. This potentially allowed for macrostructural defects leading to reduced flexural strength [50], while the properties of the microstructure are unaffected because modulus is an intrinsic property of the material and hardness is tested on a very small region. For this reason, optimization of printing parameters and toolpaths is recommended for future work.

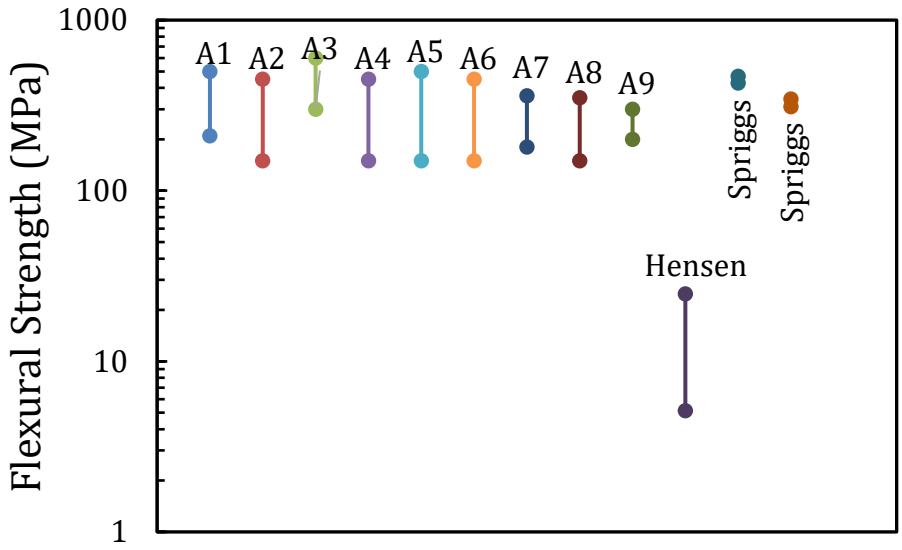

Figure 37: Flexural Strength of commercial samples as well as printed parts in this research

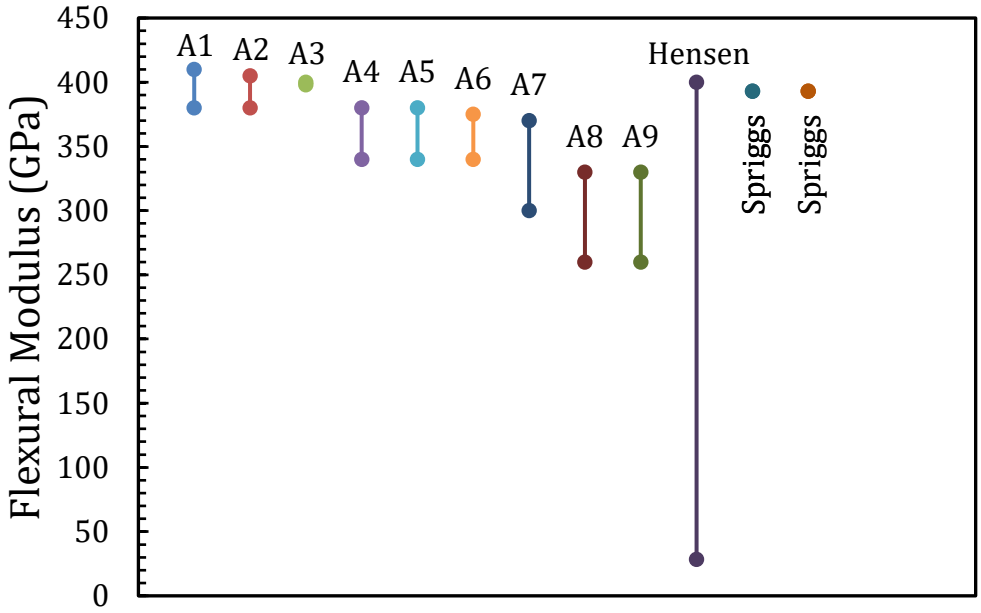

Figure 38: Flexural Modulus of commercial samples as well as printed parts in this research

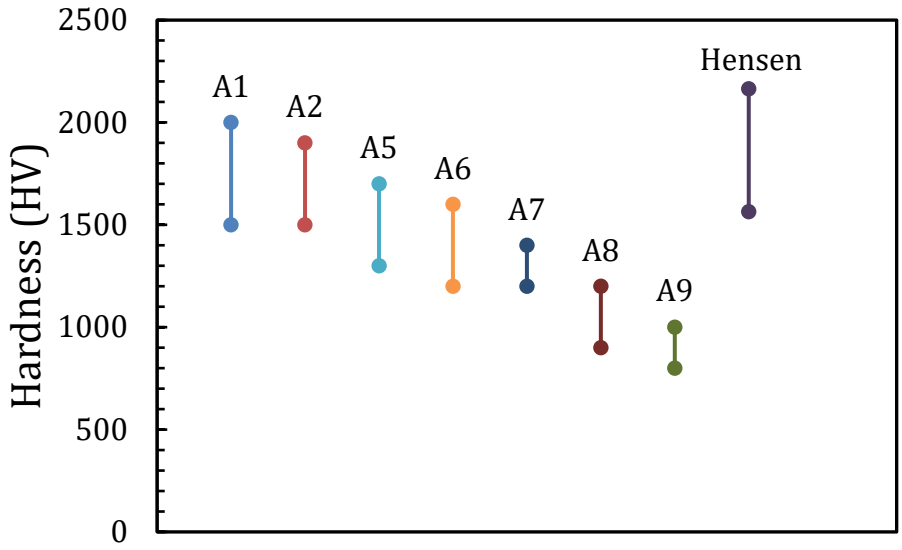

Figure 39: Hardness of commercial samples as well as printed parts in this research

3.4.5 Discussion

The method of DCP for additive manufacturing is unique and presents new advantages over conventional methods, and it has many opportunities for optimization and analysis. The analytical description of interparticle forces with respect to pH shown in Figure 29 correlates well with the observed relationship between viscosity, pH, and coagulation rate. As pH becomes more acidic, ammonia evaporation rate decreases, interparticle attractive forces are lowered, and Debye length increases, all of which contribute to a tunable suspension with higher viscosity and lower coagulation rate. However, in this study, precise control of the coagulation rate was not the goal, and clogging occurred intermittently during extrusion. This clogging can lead to complete printing failure[12], but more often leads to inconsistency in extrusion flow rate, which can lead to uneven printing. Along with this, significant flaws can arise when there is no capability to modify the extruder toolpath to mitigate staircasing, chord approximation, and perimeter overlap defects [50], as is the case with the Cura slicer engine. It is

speculated that both of these effects are a source of internal pores and flaws in what should be solid structures, such as the beams tested for flexural strength. Assuming printed parts have fracture toughness comparable to published values ($4\ MPa\sqrt{m}$)[64]–[66], internal flaw size leading to fracture at the observed stress can be calculated using Equation 12 where K_{IC} is fracture toughness, Y is a geometrical constant, σ_F is stress at failure, and a is half the length of an internal pore.

$$K_{IC} = Y\sigma_F\sqrt{\pi a}$$

Equation 12: Griffith Fracture Toughness Equation

This calculation shows that a flaw of approximately 100 μm would be sufficient to result in the observed low flexural strength. With the extruder nozzle moving at the printing speed of 10 mm/s, a flaw of this size would only require inconsistent extrusion for ~0.01 s. While hardness, flexural modulus, and translucency of samples suggest the quality of printed parts is consistent with the highest commercial grades of alumina, relatively large internal flaws due to inconsistent extrusion would account for samples breaking under relatively low loads, resulting in the low flexural strength values observed. We propose that, with more precise control of coagulation rate and extrusion flow rate, this inconsistency can very likely be mitigated. This challenge has already been observed in research and the proposed solution is not unique [50].

Once printed, a remarkable aspect of the direct coagulation technique is the relatively short cure time and complete lack of an intermediate binder burnout before sintering. Alternative methods of ceramic forming sometimes include extensive cure times for parts before they are able to be handled or sintered [12], [16], [23], [26], [27], [73]. Our method presents a significant potential decrease in production time. Many other methods

of ceramic additive manufacturing, such as binder jetting and many DIW techniques, also require removal of a binder material that may be time consuming, costly, and leave behind impurities, large pores, or cause warpage prior to sintering [3], [4], [7]. By eliminating this step, geometric fidelity, purity, and throughput time may be improved.

In the sintering process, the isotropic and consistent nature of the shrinkage can be highly advantageous to the designer. Printing with a 600 μm nozzle, parts may be oversized such that they shrink to the desired dimensions. The resulting parts have an effective resolution of approximately 486 μm. This resolution is competitive with many desktop thermoplastic FDM printers like Lulzbot, Ultimaker, Stratasys, and Makerbot, to name a few, and can likely be improved upon with higher pressure extruders or tuning of fluid properties.

For this method to be commercially viable, further characterization is necessary to generate improvements in reliability and identify suitable applications. A more thorough understanding of slurry rheology would be helpful in determining optimum printing parameters. A study of the coagulation kinetics and microstructures produced thereby could help in reducing cure time and sintering time as well as reducing clogging issues. Use of a CAD slicer program that can make continuous extrusion toolpaths with appropriate road overlap would also lower the chance of large internal flaws [50]. Further mechanical testing would be helpful in developing design parameters for parts intended for structural service. Characterization of other material properties such as electrical and thermal conductivity, and optical and wear characteristics, could validate printed parts for applications with appropriate requirements. Finally, in attempting to use direct coagulation to print with various other ceramics and metals we hope to demonstrate the true capability

of this additive method to be used across a broad spectrum of materials, many of which have not yet been shown to be printable.

3.4.6 Conclusion

A novel binderless extrusion method of additive manufacturing is presented using α-Al_2O_3 nanopowder slurries. Slurries showed good dispersion using TAC and demonstrated direct coagulation controllable with pH shift. Resulting flow and solidification properties of the slurry allowed the use of an extrusion delivery system, and the resulting 3D printed parts were sintered to full density in a single post-processing step. Coagulation is controllable so 3D printing is dependent on the kinetics of the coagulation reaction. This method is advantageous because fully dense, complex geometries can be created with little contamination, retention of small-grained microstructure, and good uniformity. The printed parts exhibited mechanical properties comparable to existing parts but with reduced strength, speculated to be caused by flaws in the toolpath or printing parameters. By further controlling the coagulation and deposition, the observed reduction in strength may be mitigated, making this method highly competitive for industrial production of structural parts. It is likely, considering the nature of alumina, that printed parts would already be suitable for research and industrial use in refractory and electrical insulation applications.

This research was funded through lab set-up funds for Dr. Troy Holland's Advanced Materials Processing and Testing (AMPT) Lab at Colorado State University. Special thanks to Dr. Qiang Wang, Dr. Matt Kipper, and Dr. Donald Radford at Colorado State University for enlightening conversations on nano-colloids, gel materials, and generosity in use of their instrumentation.

References

[1] R. M., *Sintering Theory and Practice*. 1996.

[2] J. A. Lewis, "Colloidal Processing of Ceramics," *J. Am. Ceram. Soc.*, vol. 83, no. 10, pp. 2341–2359, Oct. 2000.

[3] G. V. Franks, C. Tallon, A. R. Studart, M. L. Sesso, and S. Leo, "Colloidal processing: enabling complex shaped ceramics with unique multiscale structures," *J. Am. Ceram. Soc.*, vol. 100, no. 2, pp. 458–490, Feb. 2017.

[4] N. Travitzky *et al.*, "Additive Manufacturing of Ceramic-Based Materials," *Adv. Eng. Mater.*, vol. 16, no. 6, pp. 729–754, Jun. 2014.

[5] M. N. Rahaman, *Ceramic Processing and Sintering*, vol. Second Edition. Marcel Decker, Inc., 1995.

[6] T. Mühler, C. M. Gomes, J. Heinrich, and J. Günster, "Slurry-Based Additive Manufacturing of Ceramics," *Int. J. Appl. Ceram. Technol.*, vol. 12, no. 1, pp. 18–25, Jan. 2015.

[7] K. V. Wong and A. Hernandez, "A Review of Additive Manufacturing," *International Scholarly Research Notices*, 2012. [Online]. Available: https://www.hindawi.com/journals/isrn/2012/208760/.

[8] D. Tan *et al.*, "Reduction in feature size of two-photon polymerization using SCR500," *Appl. Phys. Lett.*, vol. 90, no. 7, p. 071106, Feb. 2007.

[9] U. Scheithauer, E. Schwarzer, A. Haertel, H. J. Richter, T. Moritz, and A. Michaelis, "Processing of thermoplastic suspensions for Additive Manufacturing of Ceramic- and Metal-Ceramic-Composites by Thermoplastic 3D-Printing (T3DP)," *Addit. Manuf. Strateg. Technol. Adv. Ceram. Ceram. Trans.*, vol. 258, pp. 19–28.

[10] U. Scheithauer, E. Schwarzer, T. Moritz, and A. Michaelis, "Additive Manufacturing of Ceramic Heat Exchanger: Opportunities and Limits of the Lithography-Based Ceramic Manufacturing (LCM)," *J. Mater. Eng. Perform.*, pp. 1–7, Aug. 2017.

[11] S. Zhao, W. Xiao, M. N. Rahaman, D. O'Brien, J. W. Seitz-Sampson, and B. Sonny Bal, "Robocasting of silicon nitride with controllable shape and architecture for biomedical applications," *Int. J. Appl. Ceram. Technol.*, vol. 14, no. 2, pp. 117–127, Mar. 2017.

[12] J. T. Muth, P. G. Dixon, L. Woish, L. J. Gibson, and J. A. Lewis, "Architected cellular ceramics with tailored stiffness via direct foam writing," *Proc. Natl. Acad. Sci.*, vol. 114, no. 8, pp. 1832–1837, Feb. 2017.

[13] D. Prawel, "Advanced/Additive Manufacturing Engineering: Principles of Extrusion," Colorado State University, 2017.

[14] J. Gonzalez-Gutierrezz, G. Stringari Beulke, and I. Emri, "Powder Injection Molding of Metal and Ceramic Parts," in *Some Critical Issues for Injection Molding*, Intech, 2012.

[15] M. Mekhail, J. Daoud, G. Almazan, and M. Tabrizian, "Rapid, Guanosine 5'-Diphosphate-Induced, Gelation of Chitosan Sponges as Novel Injectable Scaffolds for Soft Tissue Engineering and Drug Delivery Applications," *Adv. Healthc. Mater.*, vol. 2, no. 8, pp. 1126–1130, Aug. 2013.

[16] K. Prabhakaran, S. Raghunath, A. Melkeri, N. M. Gokhale, and S. C. Sharma, "Novel Coagulation Method for Direct Coagulation Casting of Aqueous Alumina Slurries Prepared Using a Poly(Acrylate) Dispersant," *J. Am. Ceram. Soc.*, vol. 91, no. 2, pp. 615–619, Feb. 2008.

[17] R. Greenwood and K. Kendall, "Selection of Suitable Dispersants for Aqueous Suspensions of Zirconia and Titania Powders using Acoustophoresis," *J. Eur. Ceram. Soc.*, vol. 19, no. 4, pp. 479–488, Apr. 1999.
[18] S. Dhara and P. Bhargava, "A Simple Direct Casting Route to Ceramic Foams," *J. Am. Ceram. Soc.*, vol. 86, no. 10, pp. 1645–1650, Oct. 2003.
[19] S. Dhara and P. Bhargava, "Influence of Nature and Amount of Dispersant on Rheology of Aged Aqueous Alumina Gelcasting Slurries," *J. Am. Ceram. Soc.*, vol. 88, no. 3, pp. 547–552, Mar. 2005.
[20] J.-H. Jean and H.-R. Wang, "Effects of Solids Loading, pH, and Polyelectrolyte Addition on the Stabilization of Concentrated Aqueous BaTiO3 Suspensions," *J. Am. Ceram. Soc.*, vol. 83, no. 2, pp. 277–280, Feb. 2000.
[21] D. J. Shanefield, *Organic Additives and Ceramic Processing: With Applications in Powder Metallurgy, Ink, and Paint*. Springer Science & Business Media, 2013.
[22] J. He *et al.*, "Dispersion of nano-sized yttria powder using triammonium citrate dispersant for the fabrication of transparent ceramics," *Ceram. Int.*, vol. 8, no. 42, pp. 9737–9743, 2016.
[23] J. Xu, Y. Zhang, Y. Qu, F. Qi, X. Zhang, and J. Yang, "Direct Coagulation Casting of Alumina Suspension from Calcium Citrate Assisted by pH Shift," *J. Am. Ceram. Soc.*, vol. 97, no. 4, pp. 1048–1053, Apr. 2014.
[24] E. E. Luther, J. A. Yanez, G. V. Franks, F. F. Lange, and D. S. Pearson, "Effect of Ammonium Citrate on the Rheology and Particle Packing of Alumina Slurries," *J. Am. Ceram. Soc.*, vol. 78, no. 6, pp. 1495–1500, Jun. 1995.
[25] Y. De Hazan, J. Heinecke, A. Weber, and T. Graule, "High solids loading ceramic colloidal dispersions in UV curable media via comb-polyelectrolyte surfactants," *J. Colloid Interface Sci.*, vol. 337, no. 1, pp. 66–74, Sep. 2009.
[26] J. A. Lewis, J. E. Smay, J. Stuecker, and J. Cesarano, "Direct Ink Writing of Three-Dimensional Ceramic Structures," *J. Am. Ceram. Soc.*, vol. 89, no. 12, pp. 3599–3609, Dec. 2006.
[27] Q. Li and J. a. Lewis, "Nanoparticle Inks for Directed Assembly of Three-Dimensional Periodic Structures," *Adv. Mater.*, vol. 15, no. 19, pp. 1639–1643, Oct. 2003.
[28] U. Scheithauer, E. Schwarzer, H.-J. Richter, and T. Moritz, "Thermoplastic 3D Printing—An Additive Manufacturing Method for Producing Dense Ceramics," *Int. J. Appl. Ceram. Technol.*, vol. 12, no. 1, pp. 26–31, Jan. 2015.
[29] X. Yan and P. Gu, "A review of rapid prototyping technologies and systems," *Comput.-Aided Des.*, vol. 28, no. 4, pp. 307–318, Apr. 1996.
[30] L. García-Gancedo *et al.*, "Application of gel-casting to the fabrication of 1–3 piezoelectric ceramic–polymer composites for high-frequency ultrasound devices," *J. Micromechanics Microengineering*, vol. 22, no. 12, p. 125001, 2012.
[31] K. Stuffle, A. Mulligan, J. Lombardi, P. Calvert, and B. Fabes, "Solid Freebody Forming of Ceramics from Polymerizable Slurry," *MRS Online Proc. Libr. Arch.*, vol. 346, Jan. 1994.
[32] R. Garg, R. K. Prud'homme, I. A. Aksay, V. F. Janas, K. S. Tenhuisen, and S. T. Huxel, "Controlled architecture ceramic composites by stereolithography," US6283997 B1, 04-Sep-2001.
[33] D. J. Wesolowski, D. A. Palmer, P. Benezeth, and L. M. Anovitz, "Surface Charge and Ion Adsorption on Metal Oxides to 290 C." Oak Ridge National Laboratory.

[34] J. O. Bockris, M. a. V. Devanathan, and K. Müller, “On the structure of charged interfaces,” *Proc R Soc Lond A*, vol. 274, no. 1356, pp. 55–79, Jun. 1963.
[35] M. A. Brown *et al.*, “Determination of Surface Potential and Electrical Double-Layer Structure at the Aqueous Electrolyte-Nanoparticle Interface,” *Phys. Rev. X*, vol. 6, no. 011007, 2016.
[36] G. Trefalt and M. Borkovec, *Overview of DLVO Theory*. 2015.
[37] B. V. Velamakanni, J. C. Chang, F. F. Lange, and D. S. Pearson, “New method for efficient colloidal particle packing via modulation of repulsive lubricating hydration forces,” *Langmuir*, vol. 6, no. 7, pp. 1323–1325, 1990.
[38] B. J. Kellett and F. F. Lange, “Thermodynamics of Densification: I, Sintering of Simple Particle Arrays, Equilibrium Configurations, Pore Stability, and Shrinkage,” *J. Am. Ceram. Soc.*, vol. 72, no. 5, pp. 725–734, May 1989.
[39] W. D. Kingery and M. Berg, “Study of the Initial Stages of Sintering Solids by Viscous Flow, Evaporation-Condensation, and Self-Diffusion,” *J. Appl. Phys.*, vol. 26, no. 10, pp. 1205–1212, Oct. 1955.
[40] U. Anselmi-Tamburini, G. Spinolo, F. Maglia, I. Tredici, T. B. Holland, and A. K. Mukherjee, “Field Assisted Sintering Mechanisms,” in *Sintering*, Springer, Berlin, Heidelberg, 2012, pp. 159–193.
[41] M. Smoluchowski, “Contribution à la théorie de l’endosmose électrique et de quelques phénomènes corrélatifs,” *Pisma Mariana Smoluchowskiego*, vol. 1, no. 1, pp. 403–420, 1924.
[42] H. A. Barnes, “Shear-Thickening (‘Dilatancy’) in Suspensions of Nonaggregating Solid Particles Dispersed in Newtonian Liquids,” *J. Rheol.*, vol. 33, no. 2, pp. 329–366, Feb. 1989.
[43] L. Bergström, “Shear thinning and shear thickening of cencentrated ceramic suspensions,” *Colloids Surf.*, vol. 133, no. 151, p. 155, 1998.
[44] C.-L. Huang, J.-J. Wang, and C.-Y. Huang, “Sintering behavior and microwave dielectric properties of nano alpha-alumina,” *Mater. Lett.*, vol. 28, no. 59, pp. 3746–3749, 2005.
[45] *Alumina - Processing, Properties, and Applications | E. Dörre | Springer*. .
[46] K. Cai, D. Guo, Y. Huang, and J. Yang, “Solid freeform fabrication of alumina ceramic parts through a lost mould method,” *J. Eur. Ceram. Soc.*, vol. 23, no. 6, pp. 921–925, May 2003.
[47] J. G. J. Peelen, “Alumina: sintering and optical properties.” Technische Hogeschool Eindhoven, 1977.
[48] C. Ladd, J.-H. So, J. Muth, and M. D. Dickey, “3D Printing of Free Standing Liquid Metal Microstructures,” *Adv. Mater.*, vol. 25, no. 36, pp. 5081–5085, Sep. 2013.
[49] J.-P. Kruth, M. C. Leu, and T. Nakagawa, “Progress in Additive Manufacturing and Rapid Prototyping,” *CIRP Ann. - Manuf. Technol.*, vol. 47, no. 2, pp. 525–540, Jan. 1998.
[50] Mukesh K. Agarwala, Vikram R. Jamalabad, Noshir A. Langrana, Ahmad Safari, Philip J. Whalen, and Stephen C. Danforth, “Structural quality of parts processed by fused deposition,” *Rapid Prototyp. J.*, vol. 2, no. 4, pp. 4–19, Dec. 1996.
[51] S. Hwang, E. I. Reyes, K. Moon, R. C. Rumpf, and N. S. Kim, “Thermo-mechanical Characterization of Metal/Polymer Composite Filaments and Printing Parameter Study for Fused Deposition Modeling in the 3D Printing Process,” *J. Electron. Mater.*, vol. 44, no. 3, pp. 771–777, Mar. 2015.

[52] P. A. Rodriguez, M. E. Bourgeois, and D. W. Radford, “Direct manufacture of continuous fiber reinforced composites through a combination of fiber placement and 3D printing,” *3rd Annu. Compos. Adv. Mater. Expo CAMX 2016*, Sep. 2016.
[53] K. M. Warlick and D. W. Radford, “Combining aspects of additive manufacture and filament winding to produce composites with novel fiber reinforcement patterns,” *3rd Annu. Compos. Adv. Mater. Expo CAMX 2016*, Sep. 2016.
[54] K. Shimamura, S. Kirihara, J. Akedo, T. Ohji, and M. Naito, *Additive Manufacturing and Strategic Technologies in Advanced Ceramics: Ceramic Transactions*. John Wiley & Sons, 2016.
[55] M. Faes, H. Valkenaers, F. Vogeler, J. Vleugels, and E. Ferraris, “Extrusion-based 3D Printing of Ceramic Components,” *Procedia CIRP*, vol. 28, pp. 76–81, Jan. 2015.
[56] J. D. Cawley, “Solid freeform fabrication of ceramics,” *Curr. Opin. Solid State Mater. Sci.*, vol. 4, no. 5, pp. 483–489, Oct. 1999.
[57] D. Guo, K. Cai, C. Nan, L. Li, and Z. Gui, “Gelcasting based solid freeform fabrication of piezoelectric ceramic objects,” *Scr. Mater.*, vol. 47, no. 6, pp. 383–387, Sep. 2002.
[58] X. Teng, H. Liu, and C. Huang, “Effect of Al2O3 particle size on the mechanical properties of alumina-based ceramics,” *Mater. Sci. Eng. A*, vol. 452, pp. 545–551, Apr. 2007.
[59] W. Miao and N. M. Zink, “Translucent alumina filaments and tape cast methods for making,” US9287106 B1, 15-Mar-2016.
[60] S. Ghanizadeh *et al.*, “Improved transparency and hardness in α-alumina ceramics fabricated by high-pressure SPS of nanopowders,” *Ceram. Int.*, vol. 43, no. 1, pp. 275–281, Jan. 2017.
[61] Z. C. Li, Z. H. Li, A. J. Zhang, and Y. M. Zhu, “Synthesis Processes of Nano Alumina Abrasive,” *Key Eng. Mater.*, vol. 368–372, pp. 691–693, 2008.
[62] H. Kanaoka, S. Kirihara, and Y. Miyamoto, “Micro-fabrication and terahetz wave properties of alumina photonic crystals with diamond structure,” *Adv. Process. Manuf. Technol. Struct. Multifunct. Mater. Ceram. Eng. Sci. Proc. Vol. 28*, pp. 99–104, 2008.
[63] T. Ohji, M. Singh, J. Salem, and D. Zhu, *Advanced Processing and Manufacturing Technologies for Structural and Multifunctional Materials: Ceramic Engineering and Science Proceedings, Volume 28*. John Wiley & Sons, 2008.
[64] R. M. Spriggs, J. B. Mitchell, and T. Vasilos, “Mechanical Properties of Pure, Dense Aluminum Oxide as a Function of Temperature and Grain Size,” *J. Am. Ceram. Soc.*, vol. 47, no. 7, pp. 323–327, Jul. 1964.
[65] P. Auerkari, *Mechanical and physical properties of engineering alumina ceramics*. Technical Research Centre of Finland Finland, 1996.
[66] R. Morrell, *Data Reviews : Section I : High-alumina Ceramics*. Crown publishers, 1987.
[67] W. H. Duckworth, C. G. Ruderer, J. F. Lynch, American Ceramic Society, and Battelle Memorial Institute, *Engineering properties of selected ceramic materials*. Columbus, Ohio: American Ceramic Society, 1966.
[68] R. M. Cannon, “Mechanical Properties of MgO and Al203,” *Am. Ceram. Soc.*, pp. 818–838, 1984.
[69] K. Cai, Y. Huang, and J. Yang, “Alumina gelcasting by using hema system,” *J. Eur. Ceram. Soc.*, vol. 25, no. 7, pp. 1089–1093, 2005.

[70] E. Ewais, A. A. Zaman, and W. Sigmund, “Temperature induced forming of zirconia from aqueous slurries: mechanism and rheology,” *J. Eur. Ceram. Soc.*, vol. 22, no. 16, pp. 2805–2812, Dec. 2002.
[71] G. R. Wiese and T. W. Healy, “Coagulation and electrokinetic behavior of TiO2 and Al2O3 colloidal dispersions,” *J. Colloid Interface Sci.*, vol. 51, no. 3, pp. 427–433, Jun. 1975.
[72] R. Laucournet, C. Pagnoux, T. Chartier, and J.-F. Baumard, “Coagulation Method of Aqueous Concentrated Alumina Suspensions by Thermal Decomposition of Hydroxyaluminum Diacetate,” *J. Am. Ceram. Soc.*, vol. 83, no. 11, pp. 2661–2667, Nov. 2000.
[73] J. Xu, N. Wen, H. Li, F. Qi, X. Xi, and J. Yang, “Direct Coagulation Casting of Alumina Suspension by High Valence Counter Ions Using Ca(IO3)2 as Coagulating Agent,” *J. Am. Ceram. Soc.*, vol. 95, no. 8, pp. 2525–2530, Aug. 2012.
[74] B. Derjaguin, “A theory of interaction of particles in presence of electric double-layers and the stability of lyophobe colloids and disperse systems,” *Acta Phys Chim*, vol. 10, pp. 333–346, 1939.
[75] B. Derjaguin and L. D. Landau, “Theory of the stability of strongly charged lyophobic sols and the adhesion of strongly charged particles in solutions of electrolytes,” *Acta Phys Chim*, vol. 14, pp. 633–662, 1941.
[76] E. J. W. Verwey and J. T. G. Overbeek, *Theory of Stability of Lyophobic Colloids*. Elsevier Amsterdam, 1948.
[77] P. Ghosh, *Interfacial Engineering: Intermolecular and surface forces*. IIT Guwahati India, 2012.
[78] T. G. Aguirre, “Effects of the addition of boron-nitride nanoplatelets to hydroxyapatite: processing, testing, and characterization.” Colorado State University, 2017.

4 Conclusion and Future Work

4.1 Conclusion

Three material systems were examined for suitability as a novel additive manufacturing method; the chitosan gel network, the PVA binder, and the direct coagulation system. Slurry preparation methods were investigated for each. After slurry evaluation, the chitosan gel method was not pursued further, as it was the least promising. Printing and sintering experiments were then performed using PVA binder and direct coagulation systems. Sintering results for the PVA binder system showed that, while printability was excellent, porosity was unacceptable. With regard to the specific aims of this research, direct coagulation printing was the only approach to demonstrate full success in extrudability, generating complex geometries, and sintering to full density. The chitosan gel network and PVA binder were simply not as easily adapted to 3D printing of complex and fully dense structures. The success of the direct coagulation approach exposes a novel, binderless, extrusion method of additive manufacturing with promise in applications with both metals and ceramics. Mixing parameters for preparation of high solids content slurries for DCP in a planetary ball mill were optimized. Sintering of DCP samples was also perfected, consistently resulting in fully dense parts. Mechanical testing of DCP printed parts was performed to allow for comparison of flexural modulus, strength, and hardness with similar alumina materials produced by conventional methods. The binderless aspect of DCP makes it more attractive than many contemporary methods by increasing potential throughput with a more time-efficient process, and simultaneously reducing cost by saving time, energy, and material investment. Ability to use nanopowders

gives the opportunity to achieve significantly better mechanical properties by producing parts with nanometric microstructural features. Overall, DCP presents a novel, binderless extrusion method of additive manufacturing, capable of using nanopowders and producing alumina parts comparable to conventionally produced alumina in mechanical properties and many contemporary printing approaches in geometric capability and speed.

4.2 Directions for Future Work

Future research efforts can be focused in two directions. First, improvements to the quality of parts can always be made; to such characteristics as resolution, strength, and repeatability in mechanical properties. Second, further applications and materials systems can be explored. Improvements in quality must come before DCP can be used for commercial applications, and demonstration of broader capabilities will enhance the range of these applications.

Proposed strategies for improving part quality are relatively direct. To improve resolution, the use of smaller extrusion nozzles is suggested. To achieve this, it is likely that some rheological optimization or increase in achievable extrusion pressure will be necessary, as viscosity and pressure are main factors in extrudability. Based on the assumption that strength of parts is reduced by slicing and extrusion errors, the first step would be to improve toolpath generation. This can either be done with commercially available programs, or by programming custom toolpaths or toolpath generation software in-house. Upon improvement of toolpaths, it is expected that part reliability can also be increased. To further improve reliability and strength, the printing environment and extrusion parameters can be optimized to eliminate nozzle clogging, providing more

consistent extrusion. With these changes implemented, it is expected that parts can be produced by DCP with acceptable quality for broad commercial applications.

DCP has been characterized in this research only for alumina powders and parts. This printing method is inherently applicable to other materials capable of electrostatic stabilization and coagulation, which includes nearly all ceramics and metals. Developing slurries and successfully creating parts with any other materials would expand the capability of industrial and research organizations involved with said material. In the biomedical sector, 3D printed implants and tissue scaffolds made of biocompatible ceramics could be produced. In the power generation and engine industry, high strength refractory metals and ceramics are of interest for ultra-high temperature heat exchangers with unique geometries only producible by AM are being researched. In space propulsion and plasma generation, complex, monolithic, and lightweight ceramics for electrical insulation are desired. These are just a few of the applications that are possible with the expansion of capability into other material systems. Similar to the evolution of thermoplastic and metal AM, there are likely many applications for AM of ceramics that have not yet been discovered. As the technology is taken up by industry and more research and experimental designs are done, there will undoubtedly be discoveries of new methods of optimizing geometry, weight, mechanical and fatigue performance, and overall application of ceramic parts. It is my hope that further research with DCP can help to advance many facets of technology in the coming years.